REPORT DOCUMENTATION PAGE

Public reporting burden for this collection of information is estimated to average 1 hour per response, including the time for reviewing instructions, searching existing data sources, gathering and maintaining the data needed, and completing and reviewing the collection of information. Send comments regarding this burden estimate or any other aspect of this collection of information, including suggestions for reducing this burden, to Washington Headquarters Services, Directorate for Information Operations and Reports, 1215 Jefferson Davis Highway, Suite 1204, Arlington, VA 22202-4302, and to the Office of Management and Budget, Paperwork Reduction Project (0704-0188), Washington, DC 20503.

1. AGENCY USE ONLY (Leave blank)	2. REPORT DATE	REPORT TYPE AND DATES COVERED
	March 1995	Final Technical 15.9.92 - 14.3.95

4. TITLE AND SUBTITLE

Efficient Pockel's Modulators in Optical Fibres

5. FUNDING NUMBERS

F49620-92-J-0480

6. AUTHOR(S)

P.G. Kazansky and P. St.J. Russell

7. PERFORMING ORGANIZATION NAME(S) AND ADDRESS(ES)

Optoelectronics Research Centre
University of Southampton
Hants. SO17 1BJ
United Kingdom

8. PERFORMING ORGANIZATION REPORT NUMBER

DTIC
ELECTE
MAY 1 2 1995
C

9. SPONSORING / MONITORING AGENCY NAME(S) AND ADDRESS(ES)

EOARD
223/231 Old Marylebone Road
London NW1 5TH
United Kingdom

10. SPONSORING / MONITORING AGENCY REPORT NUMBER

11. SUPPLEMENTARY NOTES

12a. DISTRIBUTION / AVAILABILITY STATEMENT

DISTRIBUTION STATEMENT A
Approved for public release;
Distribution Unlimited

12b. DISTRIBUTION CODE

13. ABSTRACT (Maximum 200 words)

The main aim of this project was to study the feasibility of using thermal poling of glasses as a means of realizing efficient electro-optic modulators in optical fibres. We found that substantial spreading out of the second-order nonlinearity beyond the boundaries of the positive electrode occurs, and also showed that implantation of electrons erases the second-order nonlinearity in thermally poled glass. This erasure technique holds much promise as a versatile new means of realising complex patterns for advanced electro-optic modulators. We proposed a mechanism for the thermal poling process based on a frozen-in space charge field; this model explains both our own and other recorded experimental results. Ge doping of silica glass observed to enhance both thermal poling (in combination with OH doping) and electron beam poling effects. Effective values of second-order nonlinearity as high as 0.2 pm/V were obtained in Ge-doped silica fibres. This value is ~200 times higher than ever previously reported in these optical fibres. The use of thermal poling *in vacuum* to improve in reproducibility and quality of the induced second-order susceptibility was proposed and experimentally demonstrated. Strong electro-acousto-optic transduction in thermally poled fibre was observed. Phase shift at resonance as high as 1 radian was obtained at applied fields of 0.5 V/μm. A value of electrooptic coefficient of 0.05 pm/V was experimentally measured. This value is about 25 times higher then previously reported in silica fibres and may be increased by optimisation of poling conditions.

14. SUBJECT TERMS	15. NUMBER OF PAGES
Linear electrooptic modulators, optical fibres, glass pulling, second order nonlinearities	45
	16. PRICE CODE

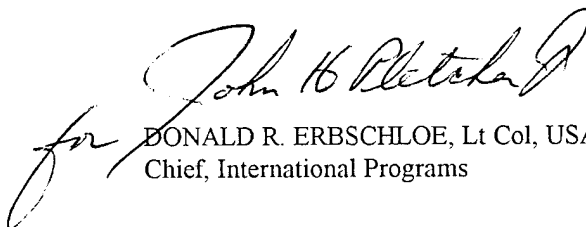| 17. SECURITY CLASSIFICATION OF REPORT	18. SECURITY CLASSIFICATION OF THIS PAGE	19. SECURITY CLASSIFICATION OF ABSTRACT	20. LIMITATION OF ABSTRACT

DTIC QUALITY INSPECTED 5

This report has been reviewed and is releasable to the National Technical Information Service (NTIS). At NTIS it will be releasable to the general public, including foreign nations.

This technical report has been reviewed and is approved for publication.

MICHAEL S. MARKOW, Lt Col, USAF
Chief, Aerospace Electronics

DONALD R. ERBSCHLOE, Lt Col, USAF
Chief, International Programs

EFFICIENT POCKEL'S EFFECT MODULATORS IN OPTICAL FIBRES
AFOSR 92-0018

Final Report — 31 March 1995

P.G. Kazansky and P.St.J. Russell

Optoelectronics Research Centre,
University of Southampton,
United Kingdom
Tel +44 703 593083/Fax +44 703 593149

19950510 044

EFFICIENT POCKEL'S EFFECT MODULATORS IN OPTICAL FIBRES

EOARD 92-0018

Final Report
31 March 1995

Contents   page

1. SUMMARY

The main aim of this project was to study the feasibility of using thermal poling of glasses (first observed in University of New Mexico) as a means of realizing efficient electro-optic modulators in optical fibres. During the first stage of the project we successfully duplicated the results of the New Mexico researchers and made a number of significant advances. Using a non-destructive method, we accurately located the position of the thermally poled layer: at a depth of 12 μm below the anodic surface. We found that substantial spreading out of the second-order nonlinearity beyond the boundaries of the positive electrode occurs, and also showed that implantation of electrons erases the second-order nonlinearity in thermally poled glass. This erasure technique holds much promise as a versatile new means of realising complex patterns for advanced electro-optic modulators. We carefully measured the ratio of nonlinear tensor elements and the polarization properties of the $\chi^{(2)}$ spatial distribution. We proposed a mechanism for the thermal poling process based on a frozen-in space charge field; this model explains both our own and other recorded experimental results. We succeeded in poling new glasses using an electron-beam poling technique. Ge doping of silica glass observed to enhance both thermal poling (in combination with OH doping) and electron beam poling effects. Effective values of second-order nonlinearity as high as 0.2 pm/V were obtained in Ge-doped silica fibres. This value is ~200 times higher than ever previously reported in these optical fibres.

During the final stage of the program, we achieved a number of significant advances in thermal poling technique of optical fibres, which allowed us to demonstrate electro-optic modulation in thermally poled optical fibre. The use of thermal poling *in vacuum* to eliminate the spreading out of the poled regions beyond the boundaries of the positive electrode was proposed and experimentally demonstrated. A substantial improvement in reproducibility and quality of the induced second-order susceptibility was achieved. A periodically modulated second-order nonlinearity was also created in optical fibre using this *vacuum* thermal poling technique. CW quasi-phase-matched frequency conversion to the blue was demonstrated. Strong electro-acousto-optic transduction in thermally poled fibre was observed for the first time. Phase shift at resonance as high as 1 radian was obtained at applied fields of 0.5 V/μm. The linear electrooptic effect in vacuum thermally poled silica fibres was measured. A value of electrooptic coefficient of 0.05 pm/V was experimentally obtained. This value is about 25 times higher then previously reported in silica fibres and may be increased by optimisation of poling conditions.

2.   WORKPLAN DESCRIPTION (extract from original proposal)

The main aim of the project is to study the feasibility of using thermal poling of doped glasses as a means of realizing efficient Pockels modulators in optical fibres. The workplan will involve the following tasks, which are summarized together with approximate time scales and levels of effort in Chart I:

Task 1:   Duplicating the New Mexico result

This initial task is aimed at reproducing the published result in bulk fused silica, in order to win the expertise needed for effective thermal poling[1]. Different samples of fused silica will be poled at a series of temperatures and the induced second order nonlinearity measured by the surface second harmonic generation (SHG) techniques to be developed in Task 5.

Task 2:   Detailed theoretical and experimental studies of field-assisted diffusive ionic transport in bulk glasses at elevated temperatures; use of this theory to confirm or refute the theory that ionic transport, leading to substantial space charge fields, lies behind the New Mexico result

The aims of this task are to develop a workable model for the glass poling mechanism, and to employ it in the design of specially doped glasses (perhaps in thin film form by rf sputtering or ion exchange techniques) in which the effect is enhanced. The ability to engineer special glasses (an ORC speciality) is perhaps the most significant ingredient of the project. Unlike in Lithium Niobate, where the Pockels coefficient is fixed by the molecular structure, in glasses its value depends on the dopants, suggesting that considerable improvements over the Myers result may be possible. A likely mechanism (not yet fully proven) is the following. It is known that, during thermal poling of glasses, charge separation caused by migration of positively charged dopant ions through glass can result in strong nonlinearities in the distribution of the electric field. Under certain conditions, most of the applied voltage is developed across a thin layer (5 μm has been reported) close to the poling anode, which is therefore subject to a very strong space charge field. Such electric fields break the macroscopic centrosymmetry of the glass, creating a second-order optical nonlinearity, permitting electric-field-induced second harmonic generation and giving rise to a non-zero Pockels coefficient whose value is proportional to the product of the third order nonlinearity and the field. By selecting glasses with higher $\chi^{(3)}$'s it may be possible to further enhance the effect, although this will be offset by lower breakdown voltages.

Task 3:   Testing of other glasses apart from silica, including glass compositions designed (from theory) to have improved poling properties

Having reproduced the New Mexico result, the experimental program will switch to new

glass compositions suggested by the modelling in Task 2. To complement the established surface SHG measurements in Task 5, techniques for testing the Pockels coefficient in bulk samples will be devised at this point.

Task 4:   Assessing the long-term stability of induced nonlinearity

The long term stability of any induced order in glasses is very important to any device application; and the easiest way of testing this involves raising the temperature. By thermally accelerating the slow changes occurring in the glass at room temperature, one can predict the lifetime of the poling effect via an Arrhenius model, which states that the rate of deterioration depends on the ratio of an activation energy to kT. The results of this Task will also feed into the design of glasses (Task 2) in which the initial poling is carried out at higher temperatures than the 250°C reported by Myers et al, and in which therefore the effect should have better long-term stability.

Task 5:   Characterization of the induced $\chi^{(2)}$ by measuring second harmonic conversion

This task will start with the setting up of a sensitive photon counting detection system (in conjunction with a Nd:YAG laser) to probe the second harmonic signal produced at the surface of the poled glass. Later on in the project the same equipment will be used for in-guide doubling in fibre (and perhaps planar if this proves useful) waveguides.

Task 6:   Characterization of the induced $\chi^{(2)}$ by direct measurement of the Pockel's coefficient

The other aspect of the induced nonlinearity is its Pockels coefficient. In a piece of material poled over a length L with an induced Pockels coefficient of r and an electrode spacing d, the voltage required for $\pi/2$ phase shift is: $V\pi/2 = \lambda d/2Ln^3r$ where n is the refractive index and λ the wavelength. Because the electrooptic index change is anisotropic, the phase shift can be converted to an amplitude change (and thus be directly detected) by incorporating the modulator into a polariser/analyses arrangement. Part of this task will be to develop a sensitive a measurement technique for bulk samples with a thin poled surface layer. In waveguide geometries the measurement is somewhat simpler, achievable experimental conditions at $\lambda = 800$ nm being $d = 5$ μm, $L = 10$ mm, $n = 1.46$ and $r = 1$ pm/V, leading to a $V\pi/2$ of 40 V. If the r coefficient can be improved by a factor of 10 by clever glass design, this could be reduced to 4 V. The highest modulation frequency of such a device (limited by the optical transition time) would be approximately $c/2nL = 5$ GHz. To improve on this, travelling wave designs could be investigated if time permits.

Task 7:   Design and fabrication of special optical fibres with core dopants and electrode systems suitable for efficient thermal poling
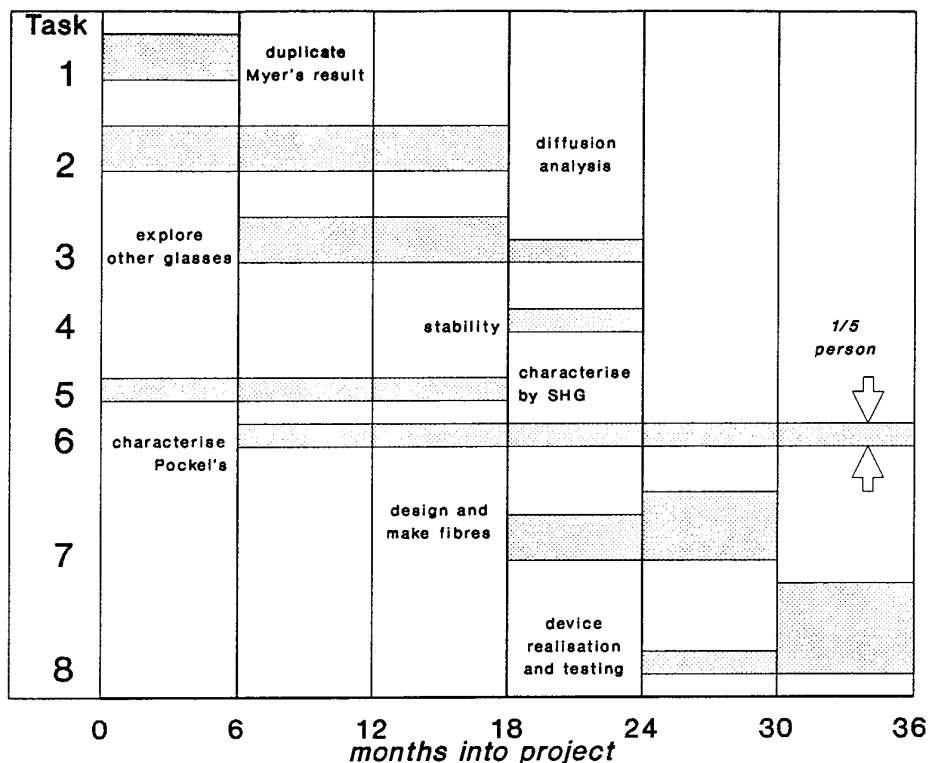
Chart I: Workplan: Durations and levels of effort of tasks

Having developed a range of glasses with optimised compositions, the next stage is to incorporate these into optical fibres with electrode systems suitable both for poling and subsequent electrooptic modulation. Dopants will be incorporated into the core by established techniques such as solution doping of the CVD deposited soot during the deposition process. The project will draw on Southampton's extensive track record in pulling fibres of D-shaped cross-section, equipped with side-channels or capillaries for incorporation of built-in metal electrodes.

Task 8: Implementation and testing of simple prototype optical fibre phase modulators and a feasibility study of their use in serrodyne frequency shifting

In this final task, a few simple prototype modulators will be built and fully characterized with a view to their being used as the basis of future development of fast electrooptic phase modulators in fibres. If there is time, a number of other devices such as a amplitude modulators (using two HiBi fibres spliced at 45° to the Pockels axis) and travelling wave phase modulators will be studied.

Milestones and deliverables

As well as quarterly reports, several milestones can be identified, including successful duplication of the Myers result after six months, a good understanding of the mechanism behind the poling effect after 18 months, together with a working model for the ionic diffusion that almost certainly lies behind the effect, and the first fibre phase modulators in the first quarter of the third year. Expected deliverables include a list of glass compositions in which the effect is optimised, some indication as to the usefulness of the poling process for SHG, and a few prototype fibre (and perhaps planar) waveguide modulators.

3. INTRODUCTION TO FINAL REPORT

3.1 Preliminary remarks

Until fairly recently second-order nonlinearities in specially treated glasses and glass fibres have been of more scientific that practical interest, owing to the small levels of nonlinearity (several orders of magnitude less than in Lithium Niobate) and their poor stability (the nonlinearity can be erased by intense infra-red or visible radiation)[2-4]. The most promising recent technique, however, is that reported by Myers and co-workers[1], who created a second-order nonlinearity of 1 pm/V (0.2 of $\chi^{(2)}(-2\omega,\omega,\omega)$ for LiNbO$_3$) by poling certain grades of commercial fused silica at 250°C under an applied electric field. This nonlinearity is extremely stable and shows no degradation under illumination with intense light. Given such a nonlinearity and taking into account its dispersion, it is possible to expect an electro-optic coefficient $r = 2\chi^{(2)}(-\omega,0,\omega)n^{-4}$ of about 1 pm/V, where n is the refractive index of silica. This value is large enough to be useful for electrooptic light modulation (the order of magnitude smaller value of nonlinearity than in LiNbO$_3$ can be compensated by a longer fibre length). This result has excited considerable interest[5-10] and stimulated the discovery of two different efficient poling techniques: Okada et al reported second harmonic (SH) generation in corona-poled glass waveguides[5] and we reported observation of about 0.7 pm/V in electron beam irradiated lead silicate glass[6]. Recently investigators from Stanford University demonstrated electro-optic phase modulation in a fused silica channel waveguide made by electron implantation[10]. A phase shift of 32 mrad was measured at λ = 633 nm for a device interaction length of 4.8 mm and an applied electric field of 7.3 V/μm. The performance of the device may be significantly improved (by a factor of 7) by increasing the spatial overlap between the nonlinearity and the modal field, which for the demonstrated device was estimated to be 0.13.

It should also be mentioned that, recently, electrooptic coefficients of about 0.3 pm/V were measured in thermally poled silica glass by a group from the University of New Mexico[23].

3.2 What are the problems of glass thermal poling?

Despite the plethora of poling techniques, the mechanisms behind the formation of the second-order nonlinearity are not fully understood. For example, Myers et al suggested that fields E_{sc} of the order of 10^7 V/cm are generated in a surface depletion region that is created near the anodic surface. This layer is depleted of cations such as Na^+ at the higher temperature, a redistribution which is frozen in by trapping as the temperature is lowered. The resulting space-charge field then creates a second order susceptibility $\chi^{(2)}$ proportional to $\chi^{(3)}E_{sc}$; this mechanism is sometimes known as electric field induced second harmonic (EFISH) generation. Although it is feasible, this mechanism does not explain the process of $\chi^{(2)}$ fixation. It is also not clear whether the high electrostatic field creates $\chi^{(2)}$ via bond orientation or via the third order susceptibility $\chi^{(3)}$. Similar questions arose in the study of photoinduced second harmonic generation in fibres, and were resolved in favour of EFISH via third-order susceptibility by experiments on the ratio of $\chi^{(2)}$ tensor components[11] and the $\chi^{(2)}$ spatial distribution[12]. In their recent work the investigators from New Mexico have suggested that bond orientation may play a dominant role[13]. They attempted to measure the distribution of second order nonlinearity using a destructive etching process; it is however difficult to relate their measurement reliably to the actual form of the nonlinearity after poling, because the removal of one layer of buried charge can strongly affect the measured nonlinearity in the whole layer. The general lack of understanding of the mechanism is closely connected with reproducibility of the results: it is clear that the poling effect is related to impurities in the glass, but the exact identity of the impurities is not clear. Without first clarifying this question, it is impossible to fabricate fibres or even glasses that reliably exhibit the effect. It is important to understand the glass poling mechanism in order to optimise the value of nonlinearity and to choose the best method for poling glass fibres. New experimental measurements on the location, polarization properties and dopant dependence of the thermally induced nonlinearity are necessary for this.

A further glass poling technique, first demonstrated by us in lead silicate glass and offering high second-order nonlinearities, is charge implantation by exposure to a low energy electron beam. This method is already in use for poling polymers[14] and creating periodically inverting domain structures in Lithium Niobate, Lithium Tantalate and KTP (reference 15-17). It has definite advantages over other poling techniques in offering the high resolution necessary for creating the complex periodic patterns needed for advanced electrooptic modulators. It was of course interesting to investigate whether this technique works also for fused silica, and whether lead silicate glass (which has high $\chi^{(3)}$) responds to thermal poling. Investigation of the interaction of the thermally poled layer with an electron beam can also help to clarify the mechanism of thermal poling effect.

4. DESCRIPTION OF WORK

During the first stage of the program, we successfully duplicated the results of the New Mexico researchers (Task 1). Using a non-destructive method, we accurately located the position of the thermally poled layer: it is at a depth of 12 μm below the anodic surface[6] (Task 5). We found that substantial spreading out of the second-order nonlinearity beyond the boundaries of the positive electrode occurs, and also showed that implantation of electrons erases the second-order nonlinearity in thermally poled glass[6] (Task 5). This erasure technique holds much promise as a versatile new means of realising complex patterns for advanced electro-optic modulators (Task 8). We carefully tested the ratio of nonlinear tensor elements and the polarization properties of the $\chi^{(2)}$ spatial distribution[7] (Task 2). We proposed a mechanism for the thermal poling process based on a frozen-in space charge field; this model explains both our own and other recorded experimental results[7] (Task 2). We succeeded in poling new glasses using an electron-beam poling technique[3] (Task 3). Ge doping of silica glass was observed to enhance both the thermal poling (in combination with OH doping) and electron beam poling effects (Task 7). Effective values of second-order nonlinearity as high as 0.2 pm/V were obtained in Ge-doped silica fibres (Task 3 and 7). This value is ~200 times higher than ever previously reported in these optical fibres (Task 7).

During the final stage of the program, we have significantly improved our thermal poling technique of optical fibres (Task 7), as proven by SHG tests of poled fibres (Task 5); we have investigated the stability of the induced nonlinearity (Task 4) and finally have succeeded in constructing a prototype all-fibre-optic electrooptic modulator (Task 8) and measuring the Pockel's effect in poled fibres (Task 6 and 8).

4.1 Duplication of New Mexico result and new results

Our experiments were carried out in a variety of different silica samples of thickness 1.3 mm and diameter 20 mm (see Table I). They were heated to about 300°C while applying a voltage of 4 kV (Figure 1). We used an oven for heating the samples in contrast to heating directly in the laboratory environment as carried out in the University of New Mexico. After some 20 minutes of poling the samples were cooled to room temperature. The dimensions of the silicon anode and the stainless steel cathode were 2 mm × 20 mm and 35 mm × 75 mm respectively, and they were pressed to the sample. After cooling to room temperature the voltage was switched off and they were removed.
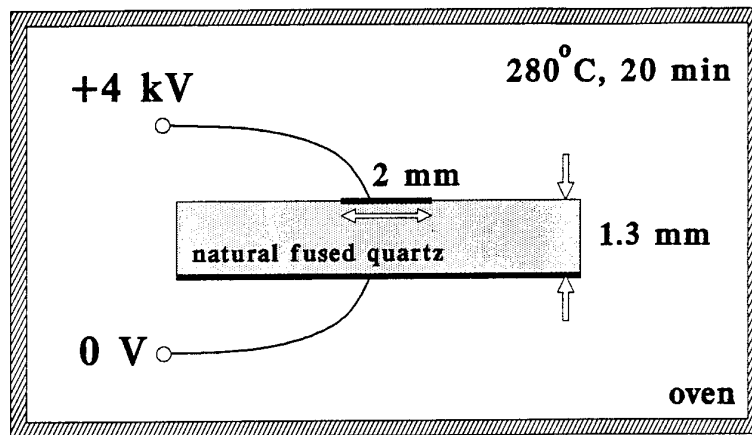
Fig. 1 Schematic diagram of the side view of the poling geometry. Silica discs of ~20 mm diameter and 1.3 mm thickness were sandwiched between the anode (2 mm × 20 mm) and the cathode.

glass type	commercial name	alkali metal (ppm)	OH (ppm)	relative SH signal
FF	Vitreosil 055	~5	~200	1
FF	Herasil 1	~4	~150	1
EF	IR Vitreosil	~4	~5	0
EF	HOQ 310	~4	~30	0.2
SS	Suprasil 2	~0.15	~1000	0.1
LS	~40 wt% PbO, several wt% Ce & TiO$_2$	—	—	0

Table I: Summary of glass types poled; FF = flame fused silica; EF = electrically fused silica; SS = synthetic silica; LS = lead silicate. An SH signal of 1 corresponds to a nonlinearity of ~1 pm/V.

Q-switched (1 kHz repetition rate, 200 ns envelope duration) and mode-locked (76 MHz

repetition rate, 3 ns pulse duration) Nd:YAG laser pulses at 1064 nm were used to probe the second order nonlinearity, with average powers of about 1.2 W. The pump laser beam (polarised in the plane of incidence) was focused by a lens (focal length 10 cm) on to the anodic surface (Figure 2). The angle of incidence (about 60°) was chosen to lie close to the Brewster angle. No SH signal was observed in the sample of IR Vitreosil, while strong
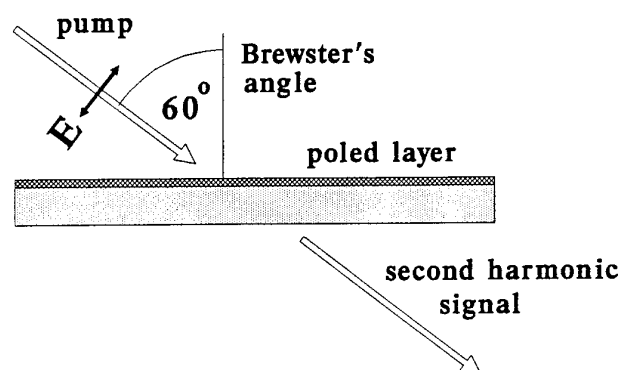

Fig. 2   Geometry used for characterising the induced second order nonlinearity.

signals of comparable strength were observed in samples of Vitreosil 055 and Herasil 1. SH signals from poled samples of Suprasil 2 and HOQ 310 were respectively 10 and 5 times less than in the above two samples. Estimated values of second-order susceptibility induced in Vitreosil 055 and Herasil 1 were respectively 1 pm/V and 0.9 pm/V; these are close to the values obtained in New Mexico. No second harmonic (SH) signal was observed in the lead silicate samples, which were treated by the thermal poling technique at a variety of different temperatures (in the range from 100°C to 350°C) at an applied voltage of 4.3 kV.

While scanning the focused laser beam along the surface of the sample in the direction perpendicular to the anode, we were surprised to observe a second harmonic signal *outside* the electrode region (Figure 3). The poled second order nonlinearity extended beyond the anode, covering an area some 1.8 times wider than the anode width. This unexpected result

in our opinion provides evidence that surface conductivity or diffusion may play role in the thermal poling process.

4.2 Erasure of thermally poled layer in silica glass by electron implantation

Additional information on the properties of the thermally poled layer in glass may be obtained by investigating the effect exposure to a focused electron beam has on the induced nonlinearity. Earlier we reported that electron implantation creates a poled layer in lead silicate glass[6]. What happens when a thermally poled layer in silica is subjected to electron implantation? A scanning electron microscope was used for irradiation of the samples. The
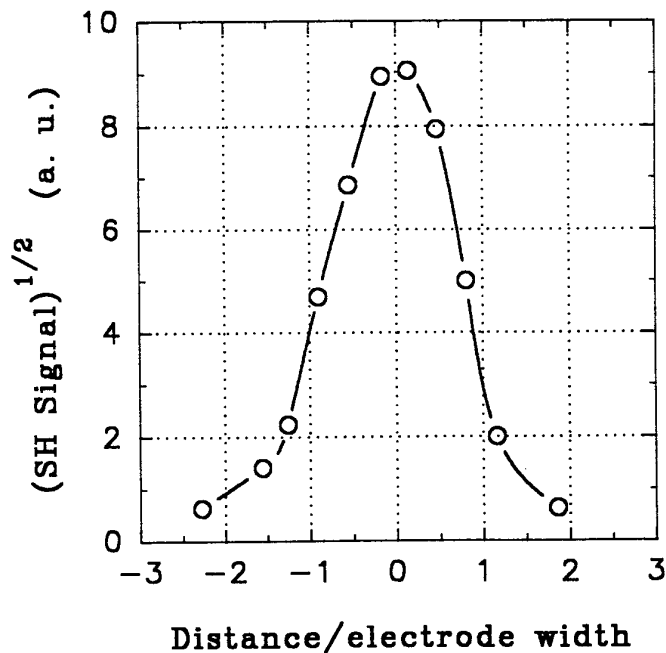

Fig. 3   Square root of SH signal versus the distance from the centre of positive electrode. The electrode width is 2 mm and the distance between the electrodes is 1.3 mm.

beam current used was 3 nA and the electron energy ranged between 5 and 40 keV. The electron beam spot size was less than 0.1 μm. The TV scanning mode of the electron microscope (horizontal scanning rate 0.064 ms/line and vertical scanning rate of 0.017 s/frame) was used. Areas of about 1 mm x 1 mm on the surface of the samples were irradiated in the electron microscope for about 1 min.

First of all, we tried to induce a $\chi^{(2)}$ by electron beam irradiation in fresh silica glass samples and some other glass structures. The results we obtained are summarised in Table II. We

Glass	$d_{33}/(d_{33}$ of doped lead glass)
F7 (lead glass)	0.4
Ge doped silica glass	0.25
Nb doped silica glass	0.1
Ti+Zr doped silica glass	0.1
lead germanate glass	0.01
phosphate glass	<0.01
synthetic silica glass	<0.01

Table II: Second order nonlinearities induced in various glasses by electron implantation, as a fraction of that obtained in Ce-doped lead silicate glass

discovered that the thermally induced $\chi^{(2)}$ was erased by the electron beam in fused silica samples. An exponential decrease of the second-order nonlinearity was observed with increasing electron-beam energy (Figure 4). A possible explanation of this erasure process runs as follows. Electrons of energy E (keV), implanted at a depth determined by the electron penetration depth R_e (μm) $= 0.018\ E^{1.75}$ (reference 14), cause neutralisation of the layer of positive charge located just near the surface. This may in some respects be similar to the etching process reported by Myers et al, which removes a charged layer from the surface. Conductivity induced by the implanted electrons might also lead to neutralisation of the frozen-in field created by thermal poling.

4.3 Non-destructive probe of poled layer distribution

For a more accurate interpretation of the experimental results it is necessary to know the distribution of nonlinearity near the surface. For this reason we cut a 1 mm thick piece from the substrate prepared by thermal poling and polished its ends. The pump beam was focused onto the butt end of the substrate and the near-field pattern of the second harmonic was imaged using a microscope objective and a video camera. The second harmonic spot was found to be localised at a depth of about 12 μm below the anodic surface and the width of
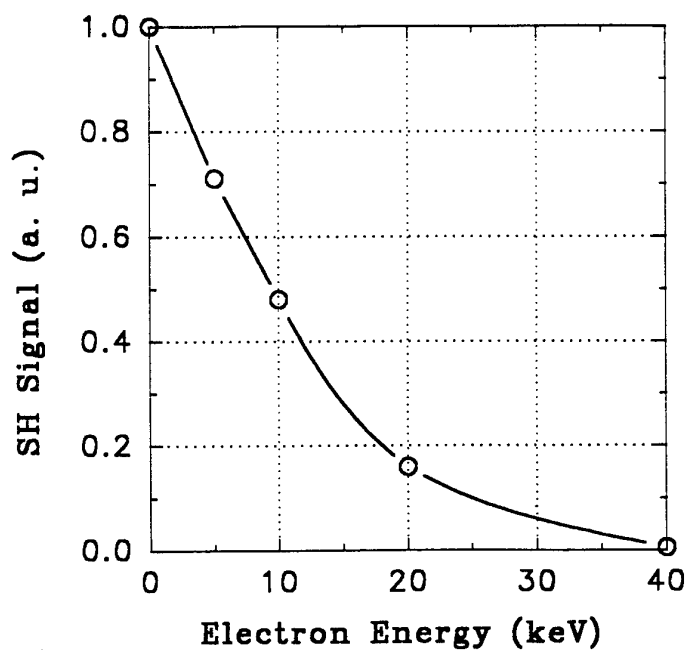
Fig. 4   SH signal from thermally poled fused silica after e-beam irradiation as a function of electron energy. The electron current and exposure time were fixed at 3 nA and 1 min respectively.

the spot was about 7 μm (Figure 5). This result is different from that obtained by Myers et
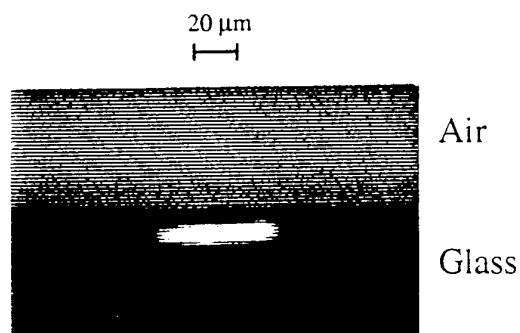
20 µm
⊢──┤

Fig. 5   SH near-field pattern in a thermally poled fused silica sample photographed from screen of the TV monitor. The nonlinearity was confined to a 7 μm wide region that was located ~12 μm below the air/glass interface.

al, who found (using a destructive etching technique) that the nonlinear layer was located just under the surface.

4.4 Thermally poled glass: frozen field or oriented dipoles?

4.4.1 Polarization properties of thermally poled layer

We also experimentally measured the ratio of the $\chi^{(2)}$ tensor components and investigated the polarization properties of the $\chi^{(2)}$ spatial distribution in thermally poled glass. A test of the proposed model of thermal poling can be made on the basis of these measurements, because a space charge field will induce a second-order susceptibility $\chi^{(2)}$ via the centro-symmetric third-order susceptibility $\chi^{(3)}$ as follows: $\chi^{(2)}{}_{ijk} = 3\chi^{(3)}{}_{ijkl}\,\mathcal{E}_l$, where $\mathcal{E}_l$ is the dc field. The components of SH polarization under these circumstances are given by:

$$P_z = \epsilon_o d_{33} E_z^2 + \epsilon_o d_{31}(E_x^2 + E_y^2)$$

$$P_y = 2\epsilon_o d_{31} E_y E_z \tag{1}$$

$$P_x = 2\epsilon_o d_{31} E_x E_z$$

where by Kleinmann symmetry the nonlinear coefficients are related by $d_{31}{:}d_{33} = 1{:}3$. In the case of dipole orientation the ratio of nonlinear coefficients will depend on whether this orientation occurs in a weak or a high field. It will be $d_{31}{:}d_{33} = 1{:}3$ in a weak field and given by the ratio of the hyperpolarizability components of the dipole in a high field. The ratio may therefore be 1:3 only for a very special dipole with this ratio of hyperpolarizability components. On the basis of the measurement of the ratio of nonlinear components, it is possible to exclude a space charge electric-field mechanism if this ratio is not close to 1:3. A ratio of exactly 1:3 will provide support an electric-field-induced mechanism, while not excluding the possibility of dipole or bond orientation. In their experiment, Myers et al measured the ratio of nonlinear coefficients in two slightly different geometries using both *p*-polarized and *s*-polarized pump beams falling on the anodic surface of the substrate. They obtained two different values - 1:7 and 1:2. This result was in favour of ordered dipoles in the poled glass. Nevertheless they could not resolve the disagreement between the two measurements.

We therefore carried out new measurements of ratio of $\chi^{(2)}$ components in an experiment with a simple geometry, where the pump propagates along the thermally poled layer (Figure 6). Silica glass samples about 1.3 mm thick were poled using the standard thermal poling procedure (280°C temperature, 4 kV applied voltage, 20 min poling duration). Q-switched and mode-locked Nd:YAG laser pulses at 1064 nm were used to probe the second order nonlinearity. A 1 mm wide piece was cut from poled substrate and two faces parallel to the direction of the applied electric field were polished. The pump beam was focused (the spot
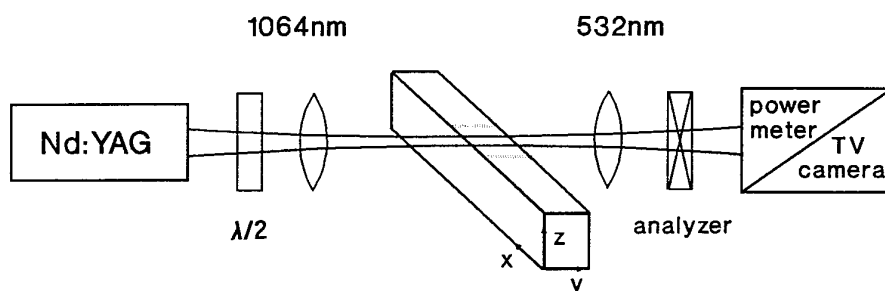
Fig. 6   Geometry used for measurement of the ratio of nonlinear coefficients.

size of the focused beam was about 50 μm) on to the butt end of the substrate and the SH signal was measured using a power meter, and its near-field intensity profile was imaged using a microscope objective and a video camera. We measured the SH signals generated by pump beams polarized perpendicular (along the z axis) and parallel (along the x axis) to the nonlinear layer. The ratio of the measured signals was about 4, yielding a ratio of nonlinear coefficients of about 2. We then analyzed the SH polarization with a Glan polarizer and were surprised to observe that it was elliptical for both cases of pump polarizations. We also observed that the near-field pattern of the SH component with polarization parallel to nonlinear layer always consisted of two or more lobes, in contrast to the near field pattern of SH component with polarization perpendicular to the nonlinear layer, which was much more uniform (Figure 7). The ratios of tensor components d_{33}/d_{31} measured with an output Glan polarizer tuned for polarization perpendicular or parallel to the nonlinear layer were 2.9 $\pm$ 0.3 and 2.8 $\pm$ 0.3. Each of these values is close enough to 3 to support a model based on a built-in space charge field.

4.4.2   Possible mechanism of thermal poling effect

On the basis of our experimental results, it is possible to explain the localisation of the nonlinearity near the anodic surface as follows. It is well-known that alkali metal ions (in particular Na^+ because of its high mobility) and H^+ are the main charge carriers in silica glass at temperatures of about 300°C. This is true in spite of the small concentration of these impurities. Under the action of the voltage applied to the heated glass, these ions will drift to the cathode where most of them are neutralised by incoming electrons, leaving behind a negatively charged *depletion region* near the anodic surface (assuming zero ionic conductivity at the anode). A high electrostatic field will then appear in the depletion region just below the anode, peaking at the interface. Assuming that all the ions that reach the cathode are neutralised, it is easy to show that in the steady-state the electric field $\mathcal{E}_0$ at the anodic
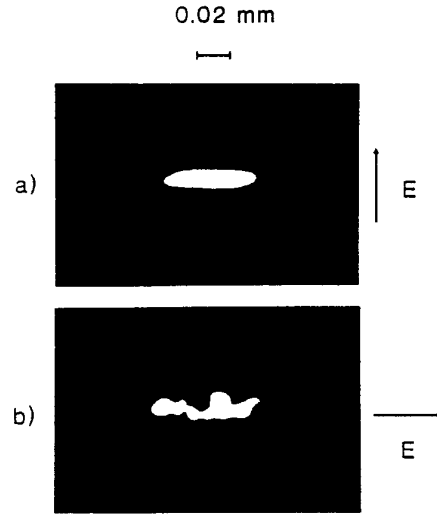
0.02 mm

Fig. 7   Second harmonic near-field intensity patterns observed for pump beams polarized perpendicular (a) and parallel (b) to the nonlinear layer; the second harmonic signal is monitored through a

interface, and the depletion region width w, are given by:

$$\mathscr{E}_o = wqN_o/\epsilon$$

$$w = \sqrt{(2\epsilon V_{app}/qN_o)}$$

(2)

where N_o is the number density of ions before poling, q their electronic charge, ϵ the dielectric permittivity and V_{app} the applied voltage. After cooling of the sample and removal of the electrodes (and assuming no extra charge build-up on the sample surface - such as positive ions attracted from the atmosphere), this field should redistribute itself to yield a zero in the centre of the depletion region. Under these circumstances, the space-charge field cannot be expected to peak consistently at 12 μm below the anodic glass surface, as experimentally observed. If, however, ionization occurs in the high field at the anode surface, electrons could flow into the anode, creating a positively charged layer within the depletion region (see Figure 8). A large frozen-in electrostatic field will then arise in the region between these two layers. This region is depleted both of H^+ ions, Na^+ ions and electrons, and will therefore have very low thermal conductivity as well as photoconductivity. The two-layered structure will be electrically neutral, which may permit the formation of a second depletion region further inside the glass; this could explain the appearance of several side lobes in the second harmonic pattern. This picture is confirmed by recent measurements we have made on the sign of the field at different surfaces on the samples. After poling at 230°C (using the electrode arrangement in Figure 2), a negative charge was left behind under the anode, whereas all other surfaces were positively charged. After poling at 280°C, however, the sample was electrically neutral, suggesting that once the depletion region is

fully developed (owing to enhanced ionic mobility at the higher temperature), breakdown occurs.
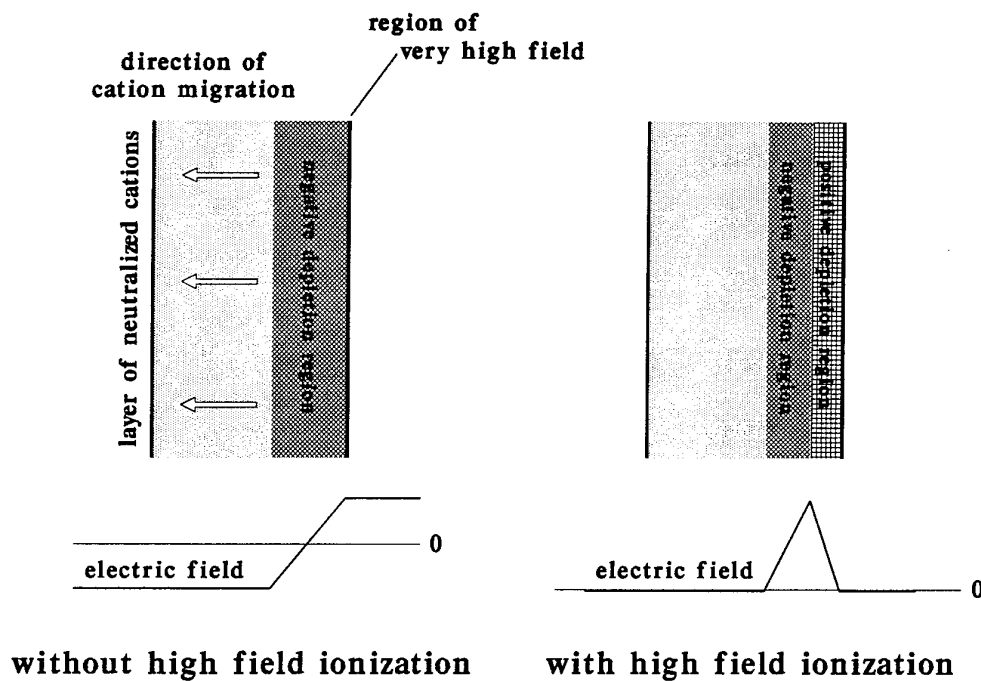

Fig. 8   The proposed mechanism of negatively-charged depletion region formation, followed by breakdown and neutralisation. The figures represent the situation after the field is turned off and the electrodes removed (the anode was on the right in each picture).

Our experiment on the measurement of the $\chi^{(2)}$ tensor components provides evidence in support of an electric-field induced $\chi^{(2)}$ model. The existence of "forbidden" field components in the second harmonic signal (i.e., those with polarization *parallel* to the nonlinear layer for pump light polarised parallel to the layer) can be explained by lateral non-uniformities in the charge distribution. Indeed, components of electrostatic field in the plane of nonlinear layer, pointing in opposite directions at each end of the non-uniform region, must arise and cause highly non-uniform distributions of second harmonic field components polarized in this plane - as observed in the our experiments (Figure 5).

4.5 High second-order nonlinearities in poled silica fibres

4.5.1 Thermal poling of fibre preforms and fibres

The lack of a clear understanding of the basic mechanisms of glass thermal poling is probably one of the main reasons why (until now) there have been no reports of successful poling of optical fibres. The maximum second-order nonlinearities, obtained by both seeding with light[2], poling with a high electrical field in germanosilicate fibres[4] and by excitation poling in P-doped germanosilicate fibres[3] remain respectively 3 orders and 1 order of magnitude lower than the thermal poling value of 1 pm/V. Using thermal poling and electron implantation techniques, we have achieved a substantial improvement in second-order nonlinearity ($\sim$200 times previous values) in germanosilicate fibres.

Fibre preforms with different compositions were thermally poled first to find the best core and cladding compositions and to understand the underlying mechanism. The preforms listed in Table III were tested.

Preform (type)	Glass tube			Inner cladding	Core
	Type	Name	OH (ppm)		
A (MCVD)	EFNQ	GE-100	$\sim$1	P+F doped silica	3.5 mol% GeO_2
B (MCVD)	FFNQ	Herasil 1	$\sim$150	P+F doped silica	18 mol% GeO_2 + Na
C (MCVD)	FFNQ	Herasil 1	$\sim$150	–	3.9 mol% GeO_2
D (MCVD)	FFNQ	Herasil 1	$\sim$150	–	4.5 mol% GeO_2 + Na
E (VAD)	–	–	$\sim$40	–	8 mol% GeO_2

Table III   Summary of fibre preforms tested by thermal poling. EFNQ = electrically fused natural quartz; FFNQ = flame fused natural quartz.

Samples approximately 1 mm thick from each preform were thermally poled at 2.5 kV applied voltage and 280 °C temperature for 15 min in an oven. Stainless steel and silicon electrodes were used.

After poling, the electrodes were removed from the samples and they were tested for evidence of second harmonic generation. Q-switched and mode-locked Nd:YAG laser operated at 1064 nm was used to probe the second-order nonlinearity. The pump laser beam was focused by a lens (10 cm focal length) on the anodic surface to a spot of about 50 μm size. The angle of incidence ($\sim 60°$) was chosen to lie close to the Brewster angle. After crossing the sample, the laser radiation was focused with a second lens on to pump and second-harmonic light detectors. Second harmonic generation in different regions of the sample was probed by traversing the sample in a direction perpendicular to the plane of incidence. No SH signal was detected in any region of preforms A and E. In contrast, a strong SH signal was observed in the flame-fused natural quartz starting tube in preforms B, C and D, and no SH signal was observed in the P+F doped cladding while scanning along preform B with a p-polarized pump (Figure 9). A small peak in SH signal was also observed at the boundary between the starting tube and the cladding with s-polarized pump. This may
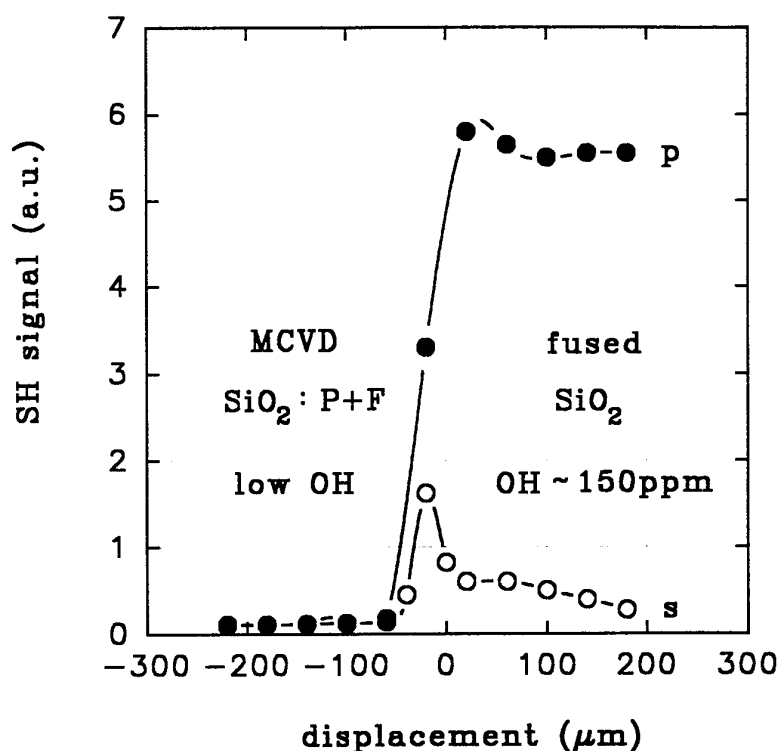

Fig. 9   SH signals for *p*-polarized pump (●) and *s*-polarized pump (○) in the cladding and starting tube in preform B.

be explained by the existence of a fringing electrostatic field at the boundary between the two regions. This has been confirmed with the observation of a peak in SH at the boundary while scanning with the pump perpendicular to the surface of the sample. We have observed ~ 15% stronger SH signal in the Ge-doped core in comparison with the starting tube (Figure 10). The SH signal in the core was also found to follow the Ge concentration in the core. In preforms C and D, we measured a high OH content in the fibre cores (~ 80 ppm).
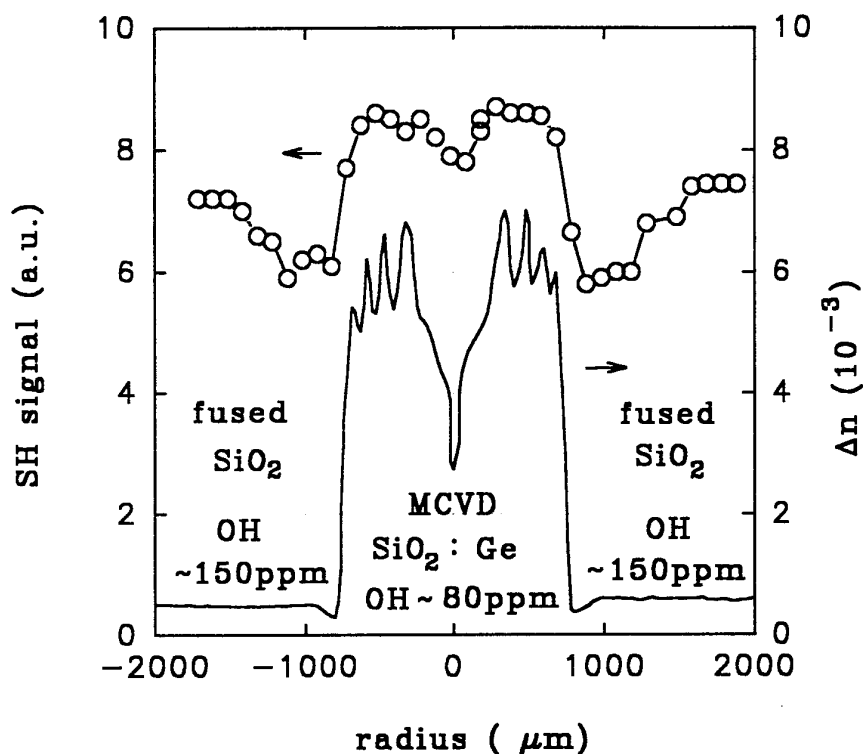

Fig. 10   SH signal (O) and refractive index difference in preform C.

Our results may be explained by a high H^+ content in the starting tubes and preform core, where they act as positively charged carriers. The observation of a higher SH signal in the Ge-doped cores may be due to Ge defect sites which can be relatively more easily ionized by the high electrostatic field in the H^+ depletion region near the anode, to create a frozen-in electric field. Interestingly, no significant effect of Na doping (preform D) on the SH signal was registered.

For the fibre poling experiments, preform B and a preform similar to preform C (GeO$_2$ concentration about 1.5 times less then in preform C) were pulled into fibre B (core diameter

2 μm, outer diameter 100 μm, numerical aperture 0.27) and fibre C (core diameter 16 μm, outer diameter 125 μm, numerical aperture 0.09) respectively. Regions ~ 8 mm long were side-polished to within about 1 μm of the core. We used a simple wheel polishing technique, which takes several minutes and induces no detectible additional loss[21]. The side-polished fibres were placed on top of a 2 mm thick silica substrate manufactured by the same method as the starting tubes (Herasil-1), and the final assembly was sandwiched between two electrodes with the anodic electrode on top of the polished fibre surface (Figure 11). Thermal poling was carried out at 4.3 kV and 280°C for 15 min.
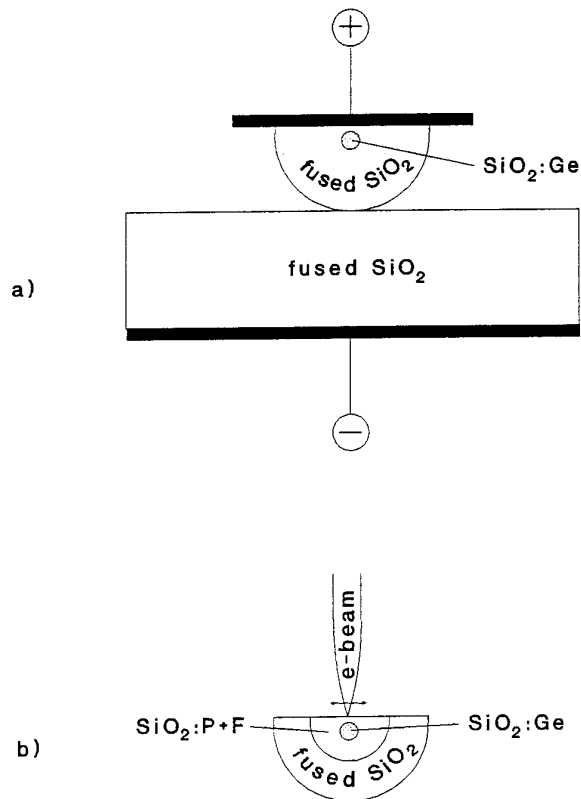

Fig. 11   Thermal (a) and electron beam (b) poling arrangements for the fibres.

After thermal poling, pump light was launched into the fibres. No SH signal was seen in fibre B. In contrast, a strong non-phasematched SH signal (visible to the naked eye) was observed in fibre C (Figure 12). We obtained a conversion efficiency of about $10^{-6}\%$ at an infrared pump of about 1 kW. Taking into account the fact that the SH signal is generated at half the coherence length ($\Lambda_{coh}/2 = 15$ μm), the effective value of the second-order
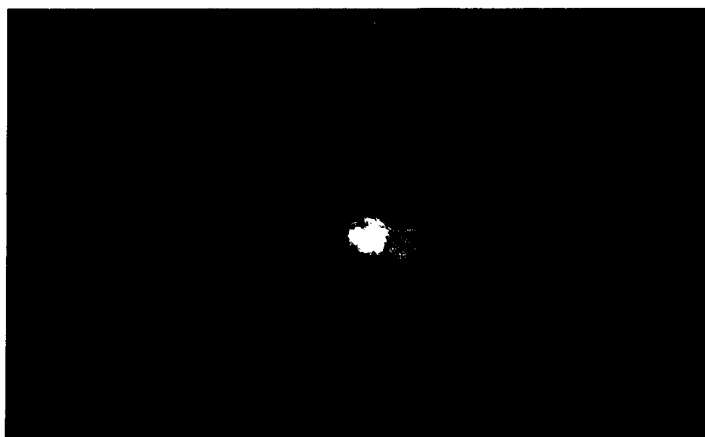
Fig. 12 Photograph of SH light generated in thermally poled germanosilicate fibre

susceptibility ($\chi^{(2)}_{eff} = \chi^{(2)}\eta$, where η is the overlap integral between the nonlinearity and the modal field) was estimated to be about 0.2 pm/V. Assuming the thickness of the nonlinear layer to be about 7 μm [7] the value of overlap factor for our fibre is $\eta \leq 0.4$, which yields the value of $\chi^{(2)} \geq 0.5$ pm/V.

4.5.2 Electron beam poling of fibres and fibre preforms

Experiments on electron beam poling were also carried out in a Ge-doped fibre preform (preform E), a side-polished Ge-doped fibre (core diameter 4 μm, outer diameter 90 μm, numerical aperture 0.3) with 22.7 mol% GeO_2, and in a pure silica sample (Suprasil). Samples were irradiated in a scanning electron microscope (SEM) at 0.3 nA beam current and 40 kV beam voltage. The TV mode of a SEM was used. Areas of about 1 mm^2 and 0.01 mm^2 on the surfaces of bulk and fibre samples (respectively) were irradiated for 1 min. After irradiation, the samples were tested for evidence of SHG using the probe technique developed for thermally poled samples. No SH signal was registered in the irradiated pure silica sample. Values of $\chi^{(2)} \simeq 0.2$ pm/V and $\chi^{(2)}_{eff} \simeq 0.1$ pm/V were obtained respectively in the core region of the Ge-doped preform and in the fibre. The result obtained using electron beam poling of Ge-doped silica can be explained by Ge-related defect centres, which act as traps for implanted electrons and also may cause an increase in secondary electron emission which finally leads to an increase in built-in electrostatic field.

4.6 Vacuum poling: an improved technique

In the fused silica thermal poling process, a ~1 mm thick sample is heated to ~250-300°C at an applied voltage of 3-5 kV. After cooling and removal of the applied field, the second-order nonlinearity is observed only near the anodic surface. This can be explained by the appearance of a high electrostatic field (of order of 10^7 V/cm) in a thin depletion region near the anodic surface[1]. We have suggested that this frozen-in electrostatic field arises between two layers of space charge near the anodic surface: a negatively charged layer depleted with cations, and a positively charged layer created by ionization in the high field between the depleted layer and the anode[19]. But some aspects of this phenomenon, such as substantial lateral spreading of the second-order nonlinearity beyond the boundaries of the positive electrode, are not fully understood. We originally suggested that this spreading is caused by the surface conductivity of the glass sample[19], and subsequently discovered that it is due to breakdown in the air surrounding the sample. Clearly, the elimination of this spreading is critical for the successful creation of quasi-phase-matched $\chi^{(2)}$ gratings and more complicated patterns for advanced electrooptic modulators. As will be clear from below, its elimination is also critical in the thermal poling of optical fibres.

4.6.1 Test of influence of surface conductivity on spreading effect

First of all, we tested the influence of surface conductivity. For this we poled two silica glass samples with different values of surface conductivity. One sample was treated before poling for about 30 min at 75°C in hexamethyldisilazane (HMDS). As a result of this, the silica surface is nearly completely covered with a monolayer of CH_3 - groups, which makes any adsorption of polar H_2O - groups very unlikely (the factor of reduction of surface conductivity is about 10^3)[20]. The other sample was not treated. After a standard thermal poling procedure (2 mm thick samples at 4.3 kV applied voltage, anode width ~2.5 mm, 280°C for 15 min), their surfaces were scanned by a focused laser beam for evidence of second harmonic generation in different regions of the samples. A mode-locked and Q-switched Nd:YAG laser operating at 1064nm was used as pump source. No difference in the spreading effect was observed between treated and untreated samples. The width of poled regions was about 1.8 times wider then the width of electrode in the both samples (Figure 13). The result of this test showed that surface conductivity is not responsible for the spreading effect.
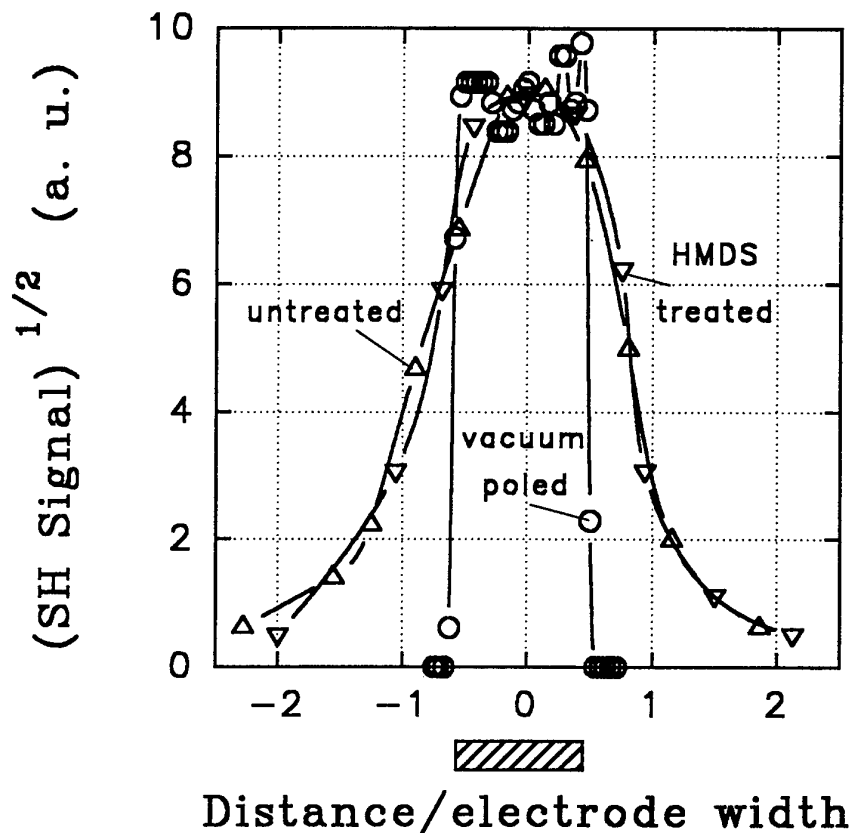
*Fig. 13   Square root of SH signal against distance from HMDS treated silica sample (▽), control sample
without any treatment (△), and vacuum poled silica sample (○).*

4.6.2   Elimination of spreading effect by vacuum poling

But another kind of conductivity exists near the anodic surface, one which may cause the spreading effect. This is conductivity due to electrical breakdown of the air. Simple estimates show that the electric field near the anode will exceed the breakdown field of air (~ 30 kV/cm), assuming a high ionic conductivity of silica glass at 280°C. In other words, air subjected to high fields near the anode acts as a very good conductor, increasing the real width of the anode. This electrical breakdown problem could of course be eliminated by poling in vacuum or possibly in some other gas or oil with a higher breakdown threshold.

We tested our suggestion experimentally. Thermal poling was carried out in an evacuated chamber at about 1.2×10^{-5} mbar. The temperature of the glass sample was raised using a radiant heater, and the poling parameters were the same as in the poling experiments in air. Second harmonic testing of the vacuum poled samples showed no evidence of spreading out of the poled regions (Figure 14). This proves that the spreading effect is caused by electrical

breakdown of the air near the anode.

4.6.3 Significant improvement of thermally poling of optical fibres by vacuum poling

We have also observed that the elimination of air leads to significant improvements in the thermally poling of optical fibres. In our fibre poling experiments we noticed that the reproducibility of the second-order nonlinearity is rather low - only of about 3% of poled fibres had a $\chi^{(2)}$ of ~ 0.2 pm/V - most had a nonlinearity an order of magnitude lower. Such poor reproducibility can be explained by electrical breakdown in the air. Indeed, we discovered that the supporting silica substrate (underneath the fibre) was also poled (Figure 14), despite there being no direct electrical contact.

To understand this, let us consider a diagram of the fibre poling arrangement, and its corresponding equivalent circuit (Figure 14). R_{d1} and R_1 are the resistances of the depletion region and the remaining fibre, R_{d2} and R_2 the resistances of the depletion region and supporting substrate and R_i is the air resistance.
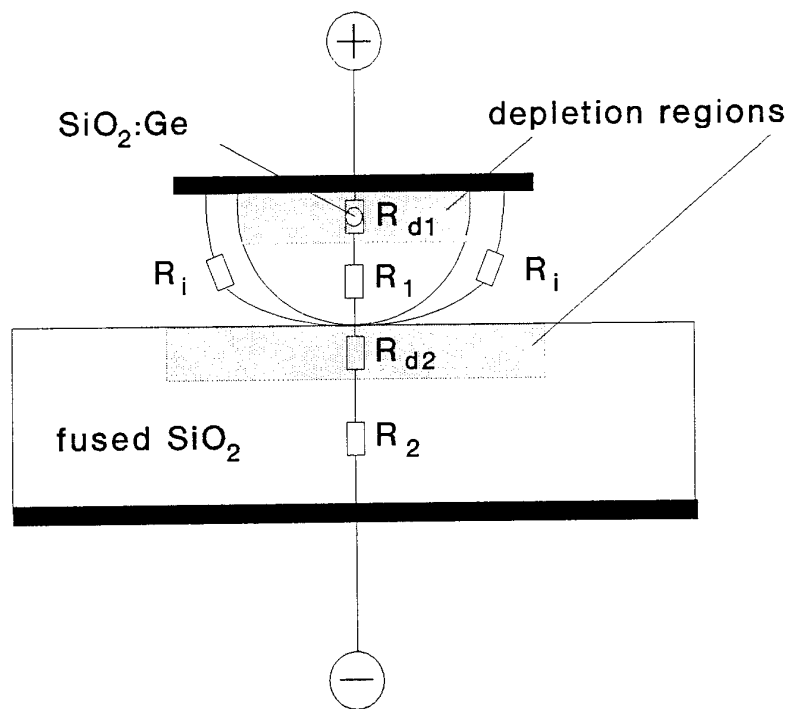

Fig. 14   Diagram of fibre thermal poling arrangement and corresponding equivalent circuit.

In the case of electrical breakdown in the air:

$$R_i \ll R_{d1}, R_1, R_{d2}; \qquad R_{d2} \gg R_{d1}, R_1, R_2 \qquad (3)$$

leading to:

$$\frac{V_{d1}}{V_{app}} \simeq \frac{R_i}{(R_{d2}+R_2)} \ll 1; \qquad \frac{V_{d2}}{V_{app}} \simeq \frac{R_{d2}}{(R_{d2}+R_2)} \simeq 1 \qquad (4)$$

which shows that only the supporting silica substrate will be poled. In the absence of air breakdown:

$$R_i \gg R_{d1}, R_1, R_{d2}, R_2; \qquad R_{d1} \gg R_{d2}, R_1, R_2 \qquad (5)$$

leading to:

$$\frac{V_{d1}}{V_{app}} \simeq \frac{R_{d1}}{(R_1+R_{d1}+R_2+R_{d2})} \simeq 1; \qquad \frac{V_{d2}}{V_{app}} \simeq \frac{R_{d2}}{(R_1+R_{d1}+R_2+R_{d2})} \ll 1$$

which shows that the poling will take place only in the fibre.

To test these predictions, we poled fibre in an evacuated chamber. Two Ge-doped fibres with fused silica cladding, numerical aperture 0.09, core and outer diameter 16 μm and 125 μm (fibre A) and respectively 6 μm and 90 μm (fibre B) were used in experiments. The cutoff wavelengths were 690 nm and 1880 nm respectively in fibre A and fibre B. The OH concentrations were 80 ppm and 150 ppm respectively in the core and in the cladding (formed from Herasil-1). Regions ~8 mm long were side-polished to within 1 μm of the core using a simple wheel polishing technique. The side-polished fibres were placed on top of 2 mm thick silica substrates, manufactured by the same method as the starting tubes (Herasil-1), and the final assembly was sandwiched between two electrodes with the anode on top of the polished fibre surface (Figure 14). The thermal poling and vacuum parameters were the same as for the bulk glass substrates.

We measured non-phase matched second harmonic generation in vacuum poled fibres. A Nd:YAG laser operating at 1064 nm was used a pump source. Second harmonic tests of the vacuum poled fibres showed almost 100% reproducibility of the value of effective second-order susceptibility $\chi^{(2)}_{eff}$ of about 0.2 pm/V ($\chi^{(2)}_{eff} = \chi^{(2)}\eta$, where η is the overlap factor between fibre mode and the nonlinearity) (Figure 15).
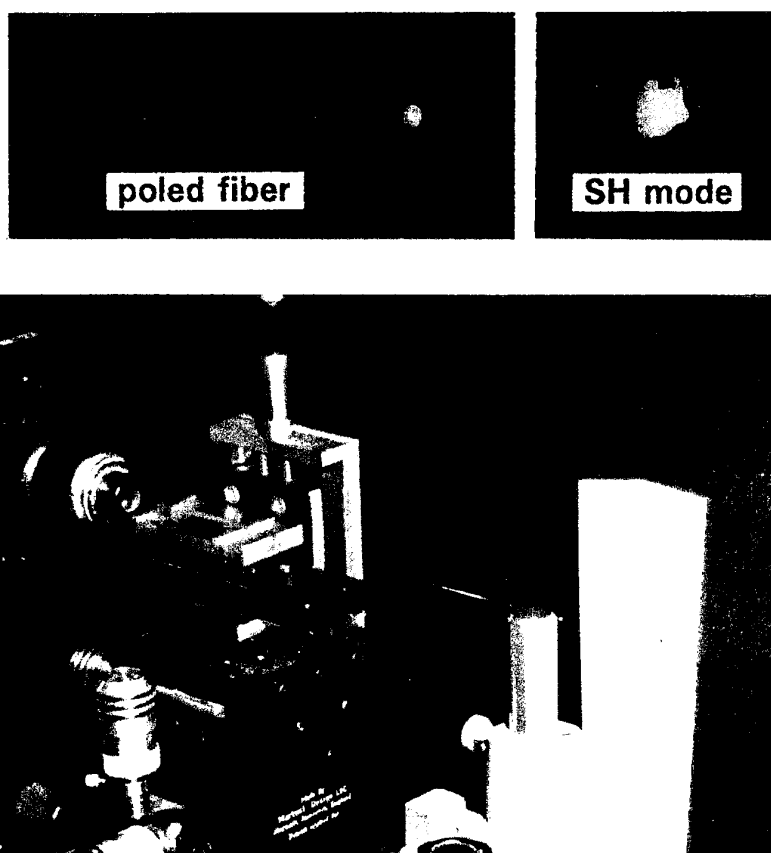
Fig.15   Photograph of second harmonic generation in vacuum poled fibre. Non-phase-matched 532 nm green
light is generated from 1064 nm IR pump.

4.7 Blue light generation in vacuum poled optical fibres

The thermal poling technique provides a means of avoiding the spreading out effect, thus
making possible the use of high resolution patterned electrodes to create complex $\chi^{(2)}$ grating
structures with uses in efficient phase-matched second harmonic generation[24] and advanced
electrooptic phase modulator design.

First of all we poled a flame-fused silica glass (Herasil 1) sample ~2 mm thick. A periodic
chromium electrode of pitch 20 μm, gap-to-finger width of 1:1, and total length of 0.7 mm,
was photolithographically patterned onto a silica (Suprasil) substrate. A periodic anode and
a uniform stainless steel cathode were simply pressed to opposite sides of the silica glass
sample. Thermal poling was carried out at 4.3 kV and 280°C for 15 min both in air and in
an evacuated chamber at 1.2×10^{-5} mbar.

After poling, the samples poled in vacuum and air were tested at 1064 nm with mode-locked and Q-switched Nd:YAG laser pulses. The near-field SH patterns were imaged on a TV monitor using a CCD camera. The on/off ratio is much better for the vacuum-poled sample, as can be seen from the photograph in Figure 16.
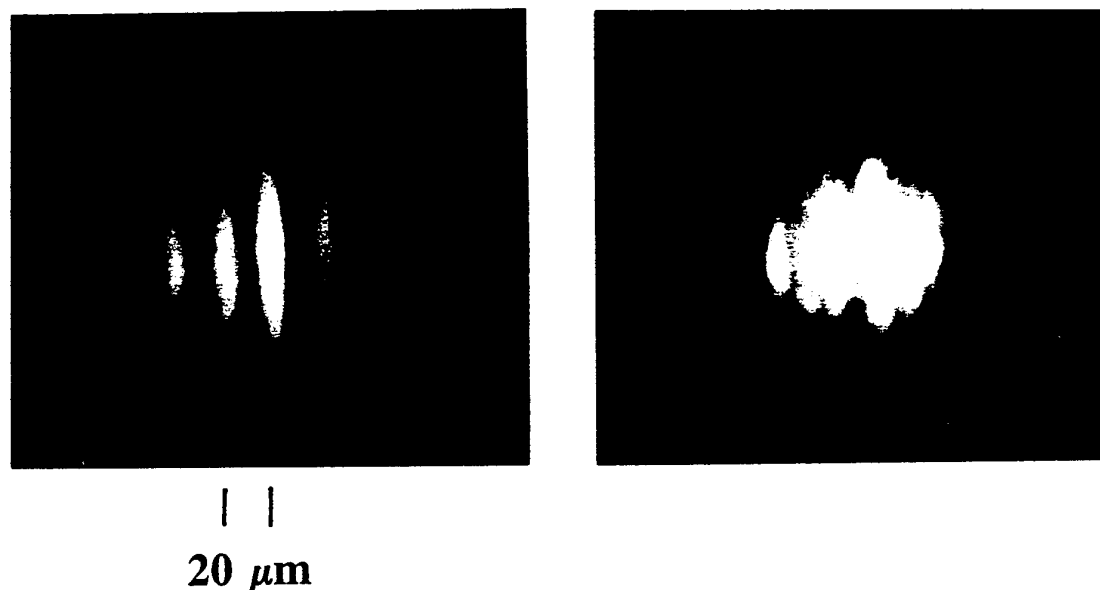

| |
20 μm

Fig. 16   Near-field second harmonic patterns in thermally poled fused silica using a periodic anode and a planar cathode in vacuum (left hand side) and air (right hand side).

Side-polished fibres A and B were also used in experiments on periodic poling of optical fibres. They were placed on top of 2 mm thick silica substrates, manufactured by the same method as the starting tubes (Herasil-1), and the final assembly was sandwiched between two electrodes with the periodic anode on top of the polished fibre surface. The thermal poling and vacuum parameters were the same as for the bulk glass substrates.

We used a CW Ti:sapphire laser with a tuning range from 780 nm to 880 nm to test the periodically poled fibres.

In order to achieve quasi-phase-matching approximately in the middle of the tuning range of the Ti:sapphire laser, it was necessary to achieve a pitch of about 28 μm. This pitch was obtained with the 20 μm period anode by tilting it through 45°. A 1 mm length of multi-mode fibre A was poled in this way.

The resulting power versus wavelength behaviour is given in Figure 17. Several phase-matching peaks are apparent. The maximum blue light detected at the peak at ~830 nm was 20 pW, corresponding to about 200 mW infrared pump in the fibre core.
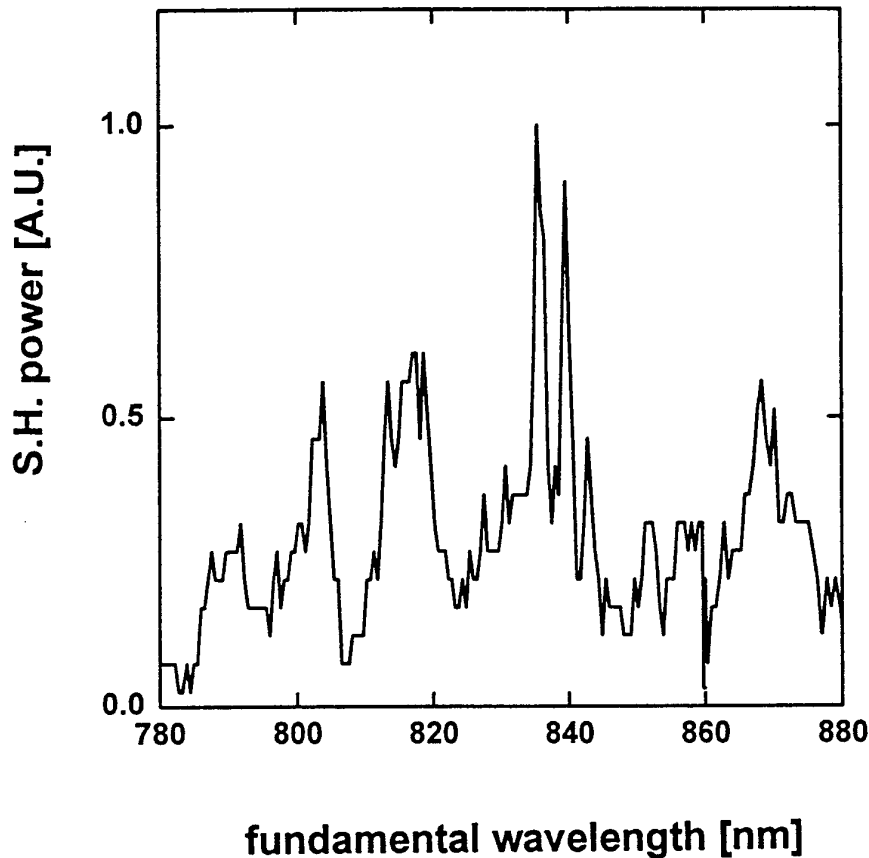

Fig. 17   Wavelength dependence of second harmonic generation in the periodically poled multi-mode fibre. Note the multiple peaks caused by modal QPM.

We used the same periodic poling technique for single-mode fibre B. A mask of pitch 28 μm and 6 mm long was used to create a grating suitable for frequency doubling of 870 nm light. The second harmonic power as a function of the fundamental wavelength is shown in Figure 18. This dependence shows a well-defined main peak of about 1.3 nm bandwidth together with small side lobes at longer wavelength. We relate the presence of the side peaks at longer wavelength to a chirp in the grating.
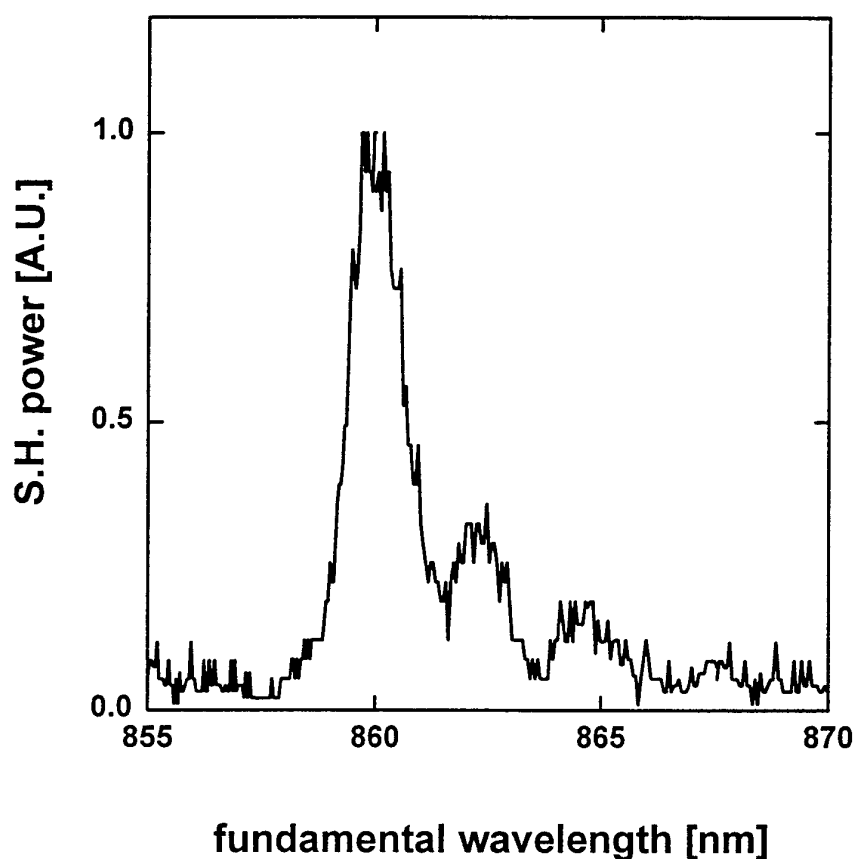
Fig. 18   Experimental dependence of the second harmonic power on the fundamental wavelength in single-mode fibre.

In Figure 19 the measured square-law dependence of the second harmonic signal on the fundamental power in the single-mode fibre is presented. The maximum blue light power detected was about 400 pW, corresponding to a fundamental power in the fibre of 100 mW. An increase of a factor about 40 in the conversion efficiency in comparison with multi-mode fibre has thus been obtained.
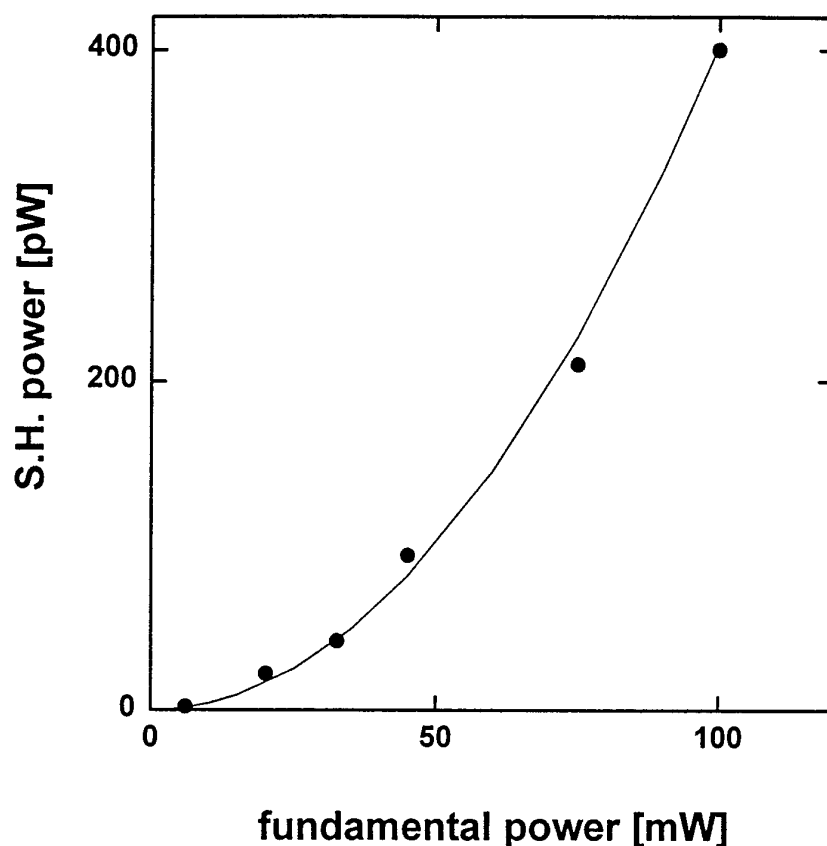
Fig. 19   Dependence of second harmonic power on pump power in single-mode fibre.

However, the effective nonlinear coefficient for the grating structure is still about 25 times lower than the value expected in a perfectly poled fibre with a nonlinearity of 1 pm/V. We believe that this reduction is related to a combination of grating imperfections (slight chirping and randomness in the length of the individual poled sections), and incomplete overlap between the poled layer and the fibre core. The presence of a chirp is suggested by the side-lobes in the phase-matching curve, all at longer wavelength with respect to the main peak. The calculated phase-matching curve obtained for a grating with a given parabolic chirp and Gaussian random fluctuations in the position of the poled regions of standard deviation of about 6.7 μm is shown in the Figure 20. As a result of these imperfections the conversion efficiency is reduced by slightly more than one order of magnitude with respect to the perfect grating. But the main reason for the small conversion efficiency, especially in the single mode fibre, is the low value of the overlap integral between the fibre modes and the poled region. The estimated value of effective nonlinear coefficient, including the overlap factor,

in the multimode fibre was about 4 times higher than the same value in the single-mode fibre, probably owing to a better overlap.
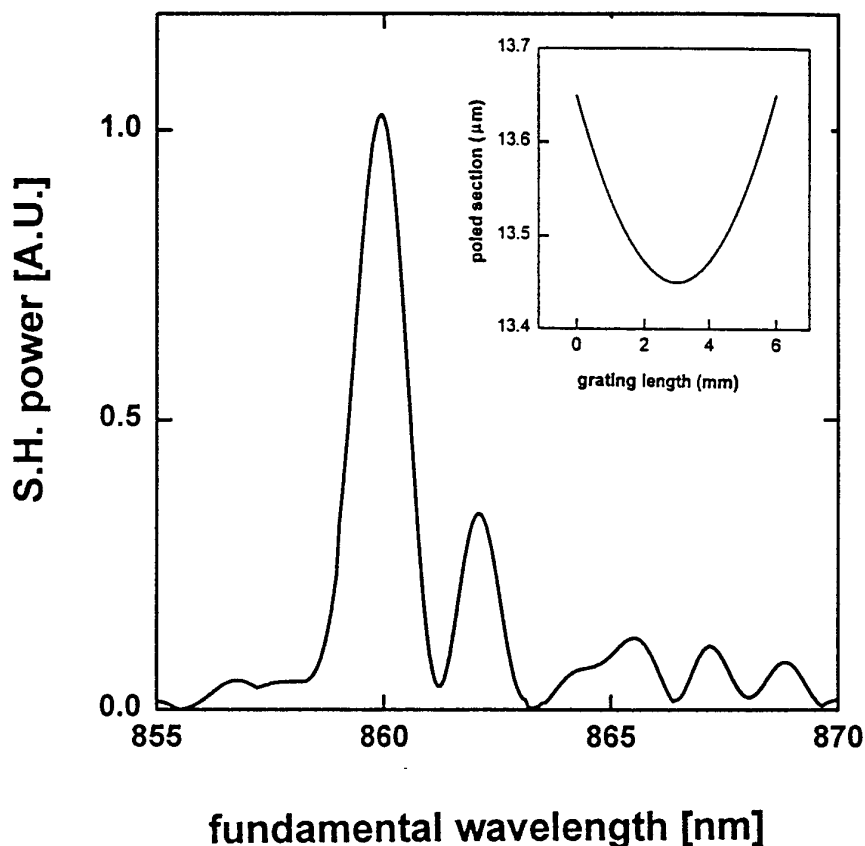

Fig. 20   Theoretical dependence of the SH power as a function of the fundamental wavelength in single-mode fibre, assuming parabolic chirp and random fluctuations of the grating.

Computer simulations of a perfect grating of 6 mm length also indicate that the experimental bandwidth of the main phase matching peak at 860 nm is very close to the predicted theoretical value of 1.3 nm (Figure 20). This indicates that the whole poled region is contributing to the SH process. The small discrepancy between the experimental and predicted phase matching wavelengths is due to the uncertainty in the Sellmeier coefficients

we used for calculating the effective refractive index of the fibre mode as a function of the wavelength. It is also worth noting that the bandwidth of phase-matched SH conversion in poled silica fibre (0.78 nm·cm) is an order of magnitude larger than in an equal length of periodically poled lithium niobate (0.06 nm·cm), owing to lower phase velocity mismatch. This may be of importance in short pulse work, where large acceptance bandwidths are required.

Considerable improvements are expected by optimization of the poling process, in particular by improving the overlap between the fundamental and SH modes within the poled region.

4.8 Interaction of poled fibre with electric field

We used fibre, thermally poled in vacuum as described above, in the experiments on the interaction of poled fibre with an electric field.

4.8.1 Estimation of the phase shift in poled fibre due to Pockel's effect

The phase shift due to the linear electrooptic effect is given by:

$$\Delta\phi \ = \ \frac{\pi n^3 rVL}{\lambda D} \tag{7}$$

where r is the electrooptic coefficient, V the applied voltage, D the gap between the electrodes and L the interaction length. This phase shift $\Delta\varphi$ is estimated to be of about 12 mrad at $r = 0.2$ pm/V, $V = 50$ V, $D = 100$ μm, $L = 8$ mm and $\lambda = 0.63$ μm.

4.8.2 Mach-Zehnder interferometer with poled fibre

A piece of fibre about 40 cm long with an 8 mm long poled region in the middle was fusion-spliced into one arm of a Mach-Zehnder interferometer made from fibres single mode at 633 nm (Figure 21). A He-Ne laser operating at 633 nm was used as the light source. A PZT phase modulator in one arm of the interferometer was used to calibrate the performance of the interferometer. Polarization controllers placed before the poled fibre were used to adjust the polarization state in the poled fibre. The poled fibre was fixed to a supporting plastic plate with one electrode underneath the poled region and a second electrode 10 mm long gently pressed to the ends of the polished region without touching the side-polished region. A signal from an ac voltage generator with frequency 0-1.5 kHz and amplitude 0-125 V was applied to the electrodes. The difference signal from the output of two silicon detectors was monitored using an oscilloscope and an RF spectrum analyzer. The operating point of the interferometer was locked by means of a control system for signal stabilization. To this end the difference signal was applied to the input of an integrator and the amplified output of the integrator used to drive a piezoelectric modulator placed in one arm of the interferometer.
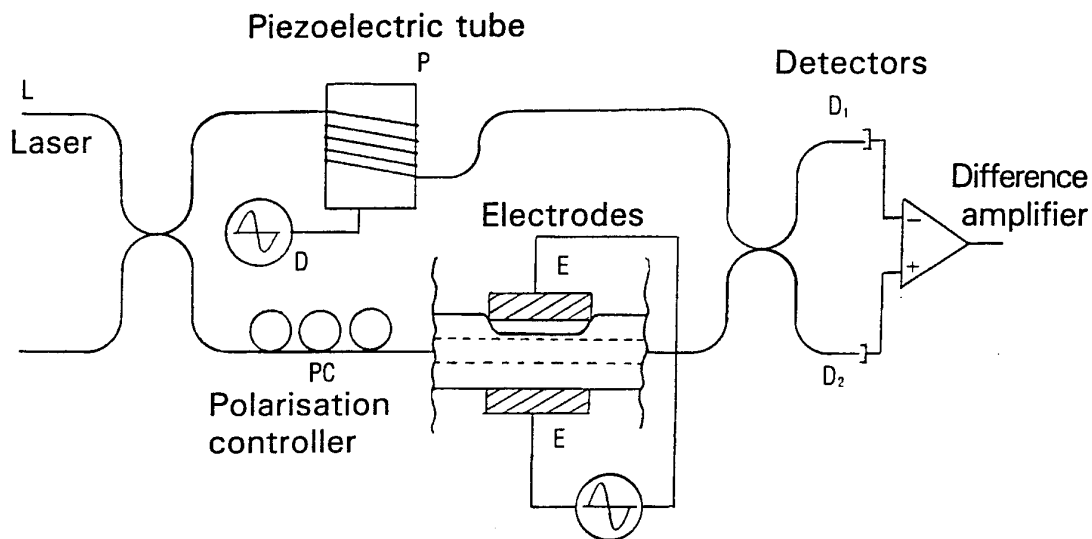
Fig. 21   Mach-Zehnder fibre-optic interferometer with poled fibre. P: piezoelectric tube; PC: polarisation controller, D: dither waveform, $D_{1,2}$: detectors, A: difference amplifier, L: laser, E: electrodes

4.8.3   Poled fibre in electrical field: observation of electro-acousto-optic transduction

We were surprised to observe a much larger phase modulation than expected by (1), together with several resonant frequencies (Figure 22).
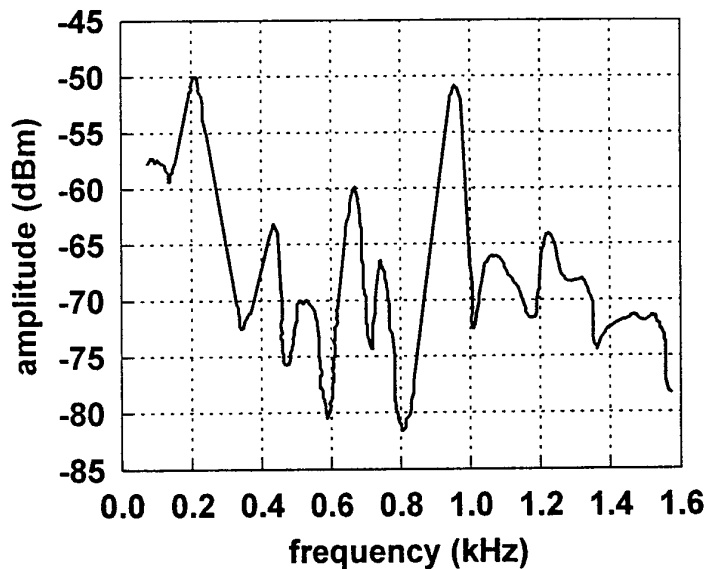

Fig. 22   Frequency dependence of interferometer output.

The output of the RF spectrum analyzer shows features typical of phase modulation (Figure 23). The largest phase shifts (~ 2 rad at 100 V peak-to-peak voltage) were measured at frequencies of 210 Hz and 950 Hz.
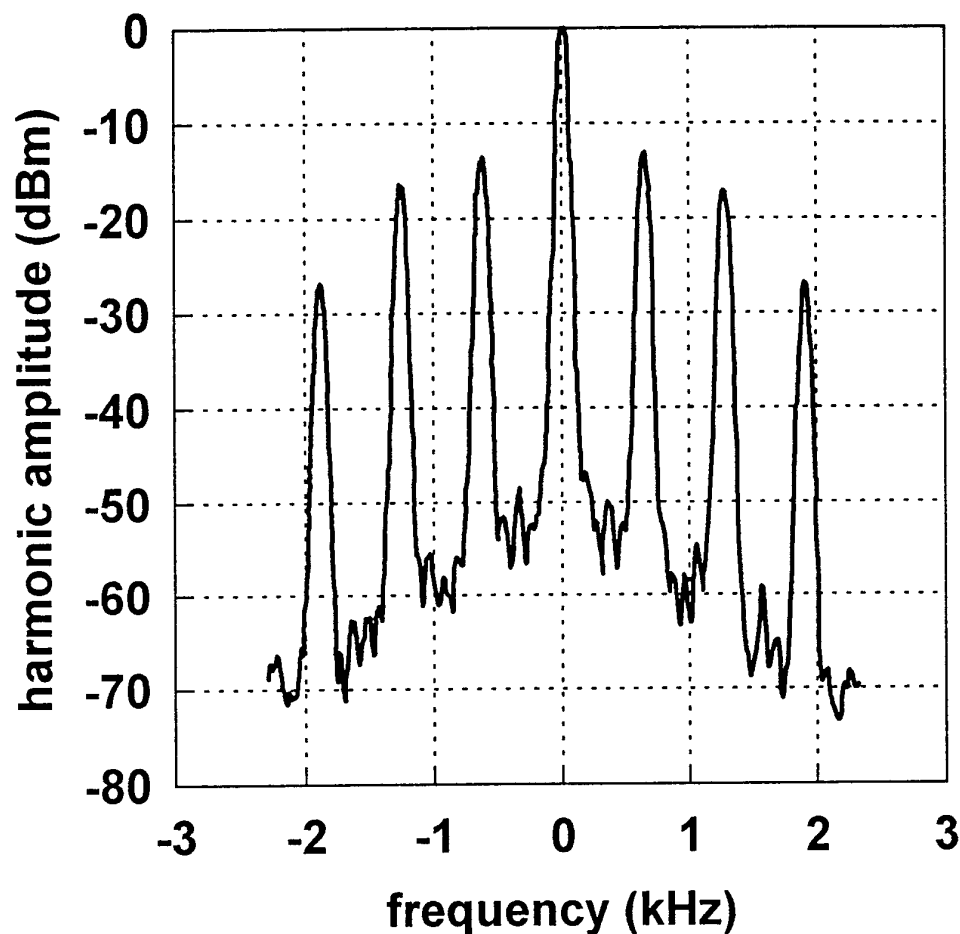

Fig. 23   Signal from interferometer output monitored on RF spectrum analyzer at applied signal amplitude 75 V and frequency 0.7 kHz.

The output signal of the interferometer was purely sinusoidal, phase-shifted relative to the applied signal: this phase shift was about $\pi/2$ at 210 Hz and about $\pi/4$ at 950 Hz (Figure 24).
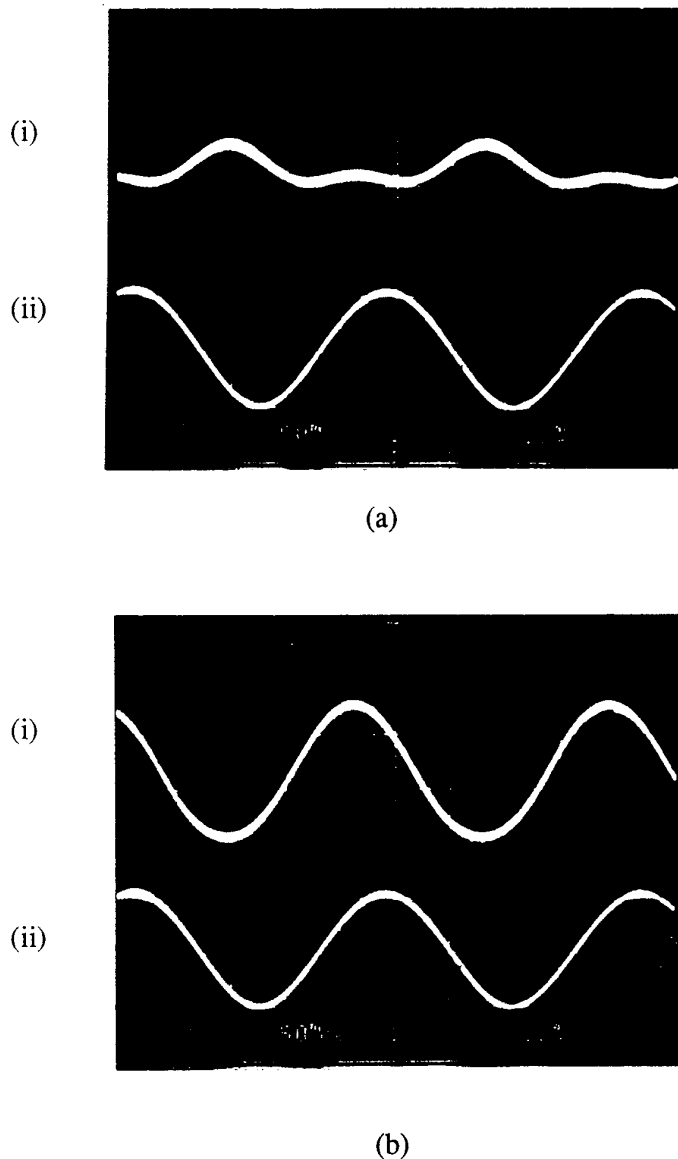
(a)

(b)

Fig. 24   Output light signal (i) and applied ac voltage (ii) at different constant phase shifts interferometer: approaching 0 (a) and about $\pi/2$ (b)

The existence of these low-frequency resonances suggests that acoustic vibrations are being excited in the system. To test this we changed the pressure of the upper electrode on the fibre and observed that the strength and position of the resonances changed. Moreover, we observed that when the upper electrode was disconnected from the voltage source the picture of phase modulation remained unchanged. This observation led us to the idea that some form of electroacoustic transduction is taking place.

4.8.4 Poled fibre in electrical field: possible explanation of experimental results

To estimate the electrostatic forces which act on the poled fibre, let us consider first of all the most probable situation, when the fibre is electrically neutral. According to our model, the thermally poled fibre has two space-charge layers of equal and opposite sign. Under these conditions, a torque $T = qdE\sin\alpha$ acts on the fibre, where E is the applied electric field inside the fibre (of radius a), α the angle between the electrical field and the dipole, d the distance between the charged layers, $q = 2E_{dip}\epsilon_o\epsilon_r La$ the charge, where $E_{dip} = \chi^{(2)}/3\chi^{(3)}$ is the space charge field in the poled layer ($E_{dip} = 1.5$ kV/μm, assuming $\chi^{(2)} = 0.5$ pm/V and $\chi^{(3)} = 10^{-22}$ m^2/V^2). Finally, the expression for the torque is as follows:

$$T = 2\epsilon_o\epsilon_r E_{dip} Lad \; \frac{V}{D} \; \sin\alpha \qquad (8)$$

and the value of torque can be estimated as about 1.7×10^{-7} Nm assuming $V = 50$ V, $d = 7$ μm, $a = 62.5$ μm, $\epsilon_r = 3.7$, $D = 100$ μm, $L = 8$ mm and $\alpha = 90°$. Such a torque is equivalent to a force of about 140 mg acting on each side of the fibre, and is sufficient to excite resonant vibrations. If the poled fibre is not electrically neutral (this can be controlled by the poling conditions[19]), electrostatic forces of the same order as those estimated above will excite transverse vibrations of the fibre. This is analogous to the behaviour of electroacoustic transducers such as those found in electret microphones and loudspeakers, and indeed the poled fibre contains an electret - a dielectric with one or more layers of space charge. In the fibre, mechanical deformations caused by electroacoustic forces produce (via the photoelastic effect) various types of isotropic and anisotropic refractive index changes in the fibre. The observed phase shift of the detected light signal relative to the applied voltage is a signature of a driven resonance.

4.8.5 Pockel's effect in thermally poled silica optical fibres: experimental results

First of all, for careful measurements of the relatively low signal from the Pockel's effect, it was necessary to eliminate the strong signal from fibre vibrations caused by electrostatic forces acting on the poled fibre. We succeeded in doing this by firmly fixing the fibre and applying uniform pressure to the poled region. The output signal from the silicon detectors - due we believe to the Pockel's effect in the poled fibre - is shown together with the applied ac voltage in Figure 25.
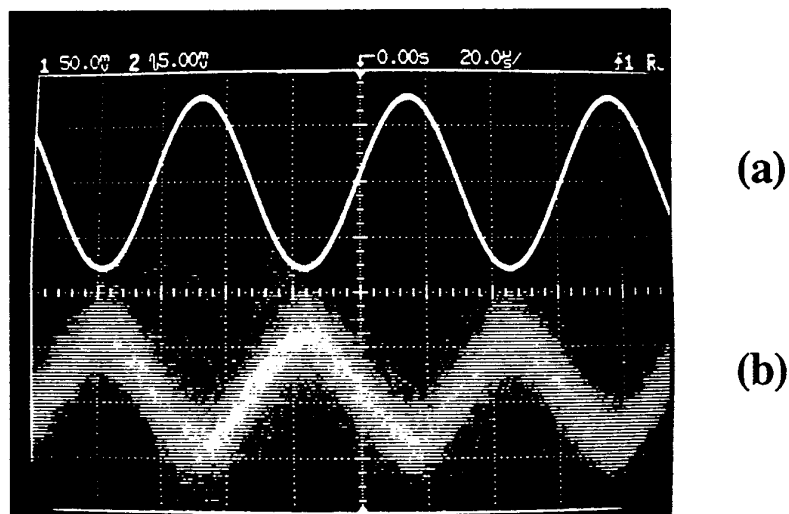
Fig. 25   Applied ac voltage (a) and output signal of Pockels modulation from silicon detectors (b) in single mode fibre. Peak-to-peak voltage is 150V.

The output signal is almost uniform in the measured frequency range up to 50 kHz and shows no evidence of acoustic resonances (Figure 26).
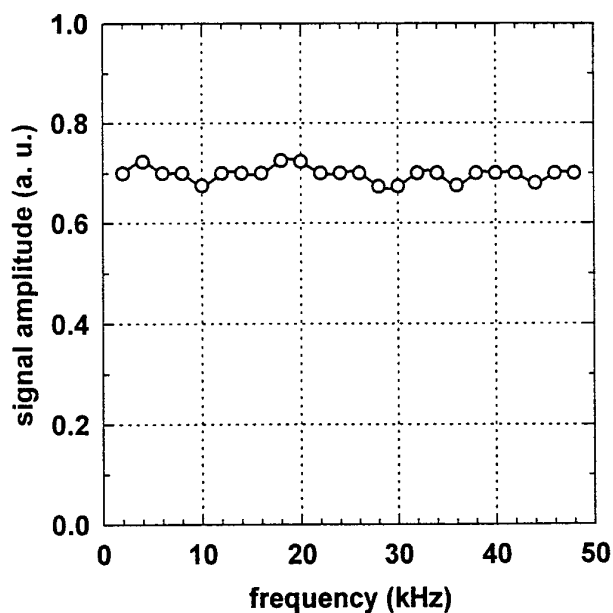

Fig. 26   Frequency dependence of electrooptic modulation.

We have measured phase shifts of about 5 mrad for a 50 μm gap in the single mode fibre (fibre A) and 3.3 mrad for a 70 μm gap in the multimode fibre (fibre B), for an applied voltage of 75 V and an electrode length of 6 mm. These measurements give a value of effective electrooptic coefficient ($r^* = r \; \eta = \Delta\phi \; \lambda \; D \; \pi^{-1} \; n^{-3} \; V^{-1} \; L^{-1}$, r - electrooptic coefficient, $\Delta\phi$ - phase shift, λ - wavelength, D - gap between electrodes, V - applied voltage, L -electrode length, η - overlap factor between poled region and fibre mode) of about 0.05 pm/V for the single mode fibre and 0.046 pm/V for the multimode fibre at 830 nm wavelength. Assuming a value of electrooptic coefficient of 0.3 pm/V [23], the value of the overlap factor is estimated to be about 0.17 for the single mode fibre A and about 0.15 for the multimode fibre B. This independence of overlap factor on Ge-doped core size can perhaps be explained by lower electrical breakdown in the Ge-doped core in the high electric field that appears near the anode surface within the negatively charged depletion region[19]. Indeed, a poled layer with a high frozen-in field can only be formed in regions with extremely low conductivity (depleted of cations as well as electrons). In the case of low electrical breakdown in the Ge-doped core, a poled layer may form only close to the lower interface between the Ge-doped region and the fused silica cladding (Figure 28).
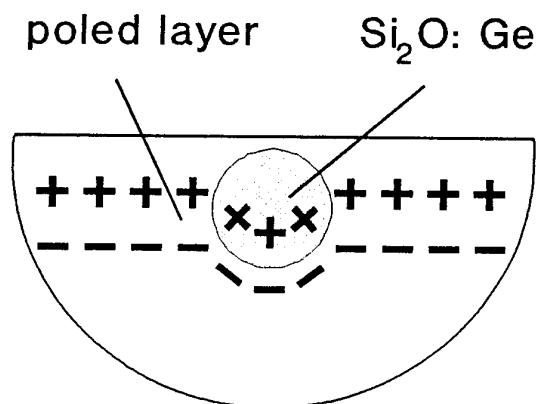

Fig. 27   Possible configuration of poled layer in the fibre with Ge-doped core.

The overlap factors may therefore be increased by optimising both the distance between the polished surface and the fibre mode, and the poling parameters themselves, e.g., poling time.

5. CONCLUSIONS

In conclusion, we have used a non-destructive method to measure the thickness of the poled layer created by thermal poling and determine its location. Substantial spreading out of second-order nonlinearity beyond the boundaries of the positive electrode is observed. This observation provides evidence that surface conductivity may play a role in the thermal poling process, which may present an obstacle to the creation of fine pitch $\chi^{(2)}$ regions using the thermal poling technique.

The erasure of the nonlinearity in the thermally poled layer by a focused electron beam has been demonstrated. This result supports the picture of a positively charged layer localised just beneath the anodic surface; it may also help to circumvent the problem of $\chi^{(2)}$ spreading. The great flexibility offered by high resolution electron-beam direct-write machines suggests that this technique may have important applications in glass-based optoelectronic devices.

The ratio of tensor nonlinear components measured using a simple arrangement, with the pump propagating along the nonlinear layer, is close to the value predicted by a model based on a frozen-in space field, but dipole orientation is not thereby completely ruled out. A mechanism for the poling effect, based on a frozen-in electrostatic field and ionization in the high field near the anodic surface is proposed. The extremely high stability of the poled layer may be explained by very low thermal and photo-conductivity due to the lack of any mobile charge carriers in the layer.

Ge-doping is observed to enhance both thermal poling (in combination with OH doping) and electron beam poling effects. Ge-related defect centres, analogous to those which cause photosensitivity in Ge-doped fibres, may be responsible for this enhancement. A value of effective $\chi^{(2)}$ as high as 0.2 pm/V is obtained in germanosilicate fibre. This value may be increased by improving the overlap between the nonlinearity and the fibre mode. Using the wheel polishing technique, fibre regions up to 3 cm may be easily side-polished and poled. Increasing the poled fibre length may be achieved either by preparation of several such regions in the same fibre, or by using D-shaped fibres. An important consequence of the work is that complex fibre geometries (different layers with different properties, small dimensions, etc) do not prevent successful application of the new poling technologies developed for planar structures.

The Pockels coefficient has been measured for the first time in vacuum-poled silica fibres. A value of about 0.05 pm/V is experimentally obtained. This is about 25 times higher then previously achieved in silica fibres[4], and may be increased at least 6 times by optimisation of the poling conditions. Large phase shifts are observed in poled fibres under an applied ac electric field. These can be explained by electro-acousto-optic transduction, and may have important practical applications for fibre optic electric field sensors at low frequencies (such

as those on electricity supply lines). The spreading-out effect in poled silica samples is caused by electrical breakdown of the air. It is effectively eliminated by poling in vacuum. Significant improvements in the thermally poling of optical fibres are also achieved if vacuum poling is used. A periodically modulated second-order nonlinearity was successfully created in optical fibre using thermal poling *in vacuo*. CW quasi-phase-matched frequency conversion to the blue is demonstrated. The measured bandwidth 0.78 nm·cm is very close to the theoretical prediction.

On the basis of these results, the main directions of construction of a practical electrooptic modulator in optical fibres are as follows:

1. Further optimization of the thermal poling conditions and fibre parameters;

2. Investigation of the possibility of increasing the induced electrooptic coefficient in glass by poling of glass structures with $\chi^{(3)}$'s higher than in silica, e.g., lead glasses by poling with short electrical pulses, or resonant enhancement of the existing $\chi^{(3)}$ in Er-doped silica glass.

A better understanding of the physical mechanisms of glass poling may lead to even higher values of electrooptic coefficient, perhaps competitive with the best electrooptic crystals.

---

6. ANCILLARY TOPICS

6.1 Publications

1. P.G. Kazansky, A. Kamal and P.St.J. Russell, "Erasure of thermally poled second-order nonlinearity in fused silica by electron implantation," Opt.Lett. **19** (693-695) 1993.

2. P.St.J. Russell, P.G. Kazansky and A. Kamal, "Electron implantation: a new poling technique for creation and modification of second order nonlinearity in glasses," SPIE *Workshop on photosensitivity and self-organisation in optical fibres and waveguides*, SPIE **2044**, paper 18, Québec City, Canada 1993.

3. P.G. Kazansky, L. Dong, P. Hua and P.St.J. Russell, "High second-order nonlinearities in poled silica fibres", in Digest of the Conference on Lasers and Electro-Optics, Anaheim, 1994, paper CFC-3.

4. P.G. Kazansky, L. Dong and P.St.J. Russell, "High second-order nonlinearities in poled silica fibres", Opt.Lett., **19**, 701 (1994).

5. P.G. Kazansky and P.St.J. Russell, "Thermally poled glass: frozen in electric field or oriented dipoles?", Optics Comm., **101**, 611 (1994).

6. P.G. Kazansky, L. Dong and P.St.J. Russell, "Vacuum poling: an improved technique for effective thermal poling of silica glass and germanosilicate optical fibres", Electron. Lett., **30**, 1345 (1994).

7. P.G. Kazansky, P.St.J. Russell and C.N. Pannell, "Optical fibre electrets and electro-acousto-optic transduction", Invited paper at the 10th Optical Fibre Sensor Conference, (Glasgow, 1994).

8. P.G. Kazansky, P.St.J. Russell and C.N. Pannell, "Optical fibre electrets: observation of electro-acousto-optic transduction", Electron. Lett., **30**, 1436 (1994).

9. P.St.J. Russell and P.G. Kazansky, "Quadratic nonlinear properties of poled glasses", in Digest of European Conference on Lasers and Electro-Optics (Amsterdam, 1994), Invited paper CTUM3.

10. P.G. Kazansky, P.St.J. Russell, L. Dong and C.N. Pannell, "Pockels effect in thermally poled silica optical fibres", Electron. Lett., **31**, 62 (1995).

11. P.G. Kazansky, V. Pruneri, O. Sugihara and P.St.J. Russell, "Blue light generation by quasi-phase-matched frequency doubling in thermally poled optical fibres", Conference on Nonlinear Optics: Materials, Fundamentals and Applications (Waikaloa, Hawaii, 1994), Post-deadline paper PD9.

12. P.G. Kazansky, V. Pruneri, O. Sugihara, L. Dong and P.St.J. Russell, "CW quasi-phase-matched second harmonic generation of blue light in poled optical fibre", to be presented at the Conference on Lasers and Electro-Optics, Baltimore, 1995.

13. P.G. Kazansky, V. Pruneri and P.St.J. Russell, " Blue light generation by quasi-phase-matched second harmonic generation in thermally poled optical fibre", to be published in Optics Letters, 1995.

6.2 Participants

Dr. P.G. Kazansky is the Research Fellow working full-time on the project. The fibres and fibre preforms are fabricated by Dr. L. Dong. Side polishing of the fibres is carried out by Mrs P. Hua using a technique that was first developed by Dr J.D. Minelly. Mr A.R. Smith has recently joined the project as a PhD student. Mr. V. Pruneri and Dr. O. Sugihara are also involved in experiments on periodically poled fibres.

6.3 Discoveries, inventions, patents

1. P.G. Kazansky and P.St.J. Russell, "A method of forming electrets in optical fibres", UK Patent Application, filed 20th April 1994.

---

7. REFERENCES

---

1. R.A. Myers, N. Mukherjee and S.R.J. Brueck, Opt. Lett. **16**, 1732 (1991).
2. U. Österberg and W. Margulis, Opt. Lett. **11**, 516 (1986).
3. M.-V. Bergot, M.C. Farries, L. Li, L.J. Poyntz-Wright, P.St.J. Russell and A. Smithson, Opt. Lett. **13**, 592 (1988).
4. L. Li and D.N. Payne in Digest of Conference on Integrated and Guided Wave Optics (Optical Society of America, Washington, D.C., 1989), paper TuAA2-1.
5. A. Okada, K. Ishii, K. Mito and K. Sasaki, Appl. Phys. Lett. **60**, 2853 (1992).
6. P.G. Kazansky, A. Kamal and P.St.J. Russell, Opt. Lett. **18**, 693 (1993).
7. P.G. Kazansky, A. Kamal and P.St.J. Russell, Opt. Lett. **19**, 1141 (1993).
8. H. Nasu, H. Okamoto, A. Mito, J. Matsuoka and K. Kamiya, Jap.J.Appl.Phys. **32**, 406 (1993).
9. K. Tanaka, K. Kashima, K. Hirao, N. Soga, A. Mito and H. Nasu, Jap.J.Appl.Phys., **32**, 843 (1993).
10. Liu, A.C., Digonnet, M.J.F., and Kino G.S., Opt. Lett., 1994, **19**, 466 (1994).
11. V. Mizrahi, Y. Hibino and G. Stegeman, Opt. Commun. **78**, 283 (1990).
12. E.M. Dianov, P.G. Kazansky, D.S. Starodubov and D.Yu. Stepanov, Sov. Lightwave Commun. **2**, 83 (1992).
13. N. Mukherjee, R.A. Myers and S.R.J. Brueck, in Digest of Conference on Lasers and Electro-Optics (Optical Society of America, Washington, D.C., 1993), paper CThP4
14. B. Gross, in *Electrets*, G.M. Sessler, ed. (Springer-Verlag, Berlin, 1980), Chapter 4.
15. H. Ito, C. Takyu and H. Inaba, Electron. Lett. **27**, 1221 (1991).
16. W.-Y. Hsu and M.C. Gupta, Appl. Phys. Lett. **60**, 1 (1992).
17. M.C. Gupta, W.P. Risk, A.C.G. Nutt and S.D. Lan, **60**, (1993).
18. Y.L. Xue, P.L. Chu and W. Zhang, J.Opt.Soc.Am. **B**, 1840 (1993).
19. Russell, P.St.J., Kazansky, P.G., and Kamal, A., SPIE **2044**, 192 (1993).
20. Voorthuyzen, J.A., Keskin K., and Bergveld, P., Surface Science, **187**, 201 (1987).
21. Hussey, C.D., and Minelly, J.D., Electron. Lett., **24**, 805 (1988).
22. Li,L., and Payne D.N.:"Permanently-induced linear electrooptic effect in silica optical fibres", in Digest of Conference on Integrated and Guided Wave Optics (Optical Society of America, Washington, D.C., 1989), paper TuAA2-1.
23. Long, X-C., Myers, R.A., and Brueck, S.R.J., Opt. Lett., **19**, 1819 (1994).
24. Kashyap, R., Veldhuis, G.J., Rogers, D.C. and McKee, P.F., Appl. Phys. Lett., **64**, 1332 (1994).